Measuring Conflict in Multi-Objective Optimization: A Case Study of the Impact of Climate Change on the Joint Provision of Forest Ecosystem Services

Nicholas D. C. Kullman

A thesis
submitted in partial fulfillment of the
requirements for the degree of

Master of Science

University of Washington

2016

Committee:

Sándor F. Tóth, Chair

David Butman

W. Art Chaovalitwongse

Program Authorized to Offer Degree:
Quantitative Ecology and Resource Management

University of Washington

Abstract

Measuring Conflict in Multi-Objective Optimization:
A Case Study of the Impact of Climate Change on
the Joint Provision of Forest Ecosystem Services

Nicholas D. C. Kullman

Chair of the Supervisory Committee:
Associate Professor Sándor F. Tóth
School of Environmental and Forest Sciences

We present here a novel process to measure the conflict within and across multi-objective systems. To do so, we propose a new metric to quantify pairwise objective conflict. We also provide new applications for two existing measures of conflict from evolutionary multi-objective optimization (EMO). To demonstrate the utility of our proposed conflict measure and our conflict quantification process, we conduct a case study of the impact of climate change on the joint provision of forest ecosystem services. For each of three climate scenarios, we quantify the total amount of conflict in the multi-objective system and we also compare the conflict across climate scenarios.

Our results show that our proposed process and the new conflict metric are successful at quantifying and differentiating the amount of conflict within and across multi-objective systems and that they stand to serve as a useful tool for multi-objective decision making.

TABLE OF CONTENTS

LIST OF FIGURES

LIST OF TABLES

ACKNOWLEDGMENTS

My first thanks go to Sándor Tóth, David Butman, and Art Chaovalitwongse for their advising of this research. A special thanks goes to Sándor for his emphasizing my personal growth as a graduate student and for constantly reminding me of the big picture. I also want to thank Svetlana Schroder for introducing me to the project and her continued support throughout. I would also like to acknowledge all those who contributed to the tools or data used in this study, such as Heather Roberts with the LEMMA team at Oregon State University; Bill Elliot from the US Forest Service's WEPP team; Mike, Lance, and others with the FVS and Climate-FVS teams; the developers for CPLEX, D3, and pandas; and many others. I also want to thank those who have funded my graduate research, including QERM, the Precision Forestry Cooperative, and the US Forest Service.

I would also like to thank my labmates and fellow QERMies for acting as sounding boards and for many good times at soup. Finally, my most heartfelt thanks to my family – to my parents and grandparents for instilling in me the importance of curiosity and education, and to my wife, whose endless moral (and financial) support has made my graduate education possible.

DEDICATION

To Rachel, my parents and grandparents

Chapter 1

MEASURING CONFLICT IN MULTI-OBJECTIVE OPTIMIZATION: A CASE STUDY OF THE IMPACT OF CLIMATE CHANGE ON THE JOINT PROVISION OF FOREST ECOSYSTEM SERVICES

1.1 Introduction

Many tasks in resource allocation are multi-objective. The design of aircraft involves balancing cost and efficiency [25]. Hospitals seek to manage personnel and equipment in order to maximize patient throughput while minimizing cost and required back-up [13]. Food production balances processing time with nutrient retention [21]. Forest managers aim to provide carbon sequestration and wildlife habitat while also maximizing timber revenues [23].

Given a set of solutions to one of these resource allocation problems, a decision maker chooses one to enact. Often, no one solution simultaneously optimizes all objectives, and the decision maker must therefore choose a solution that represents a preferred compromise among them. In such cases, there is some amount of conflict among the objectives. This is in contrast to compatible or harmonious objective relationships in which the objectives improve simultaneously.

In the case of aircraft design, cost and efficiency conflict with one another, since more efficient design details tend to cost more. Similarly, hospitals may increase patient throughput by increasing the number of doctors available, but this decision would increase costs. Food production engineers can maximize nutrient retention by reducing the temperature at which processing occurs, but this would lengthen the time required to reach acceptable microbiological levels. Forest managers can maximize timber revenue by removing large old-growth forest, but this would reduce the available wildlife habitat.

While the preferred solution may vary by decision maker, a rational decision maker will always prefer one which is Pareto efficient; that is, a solution in which no objective can be improved without compromising another. Multi-objective optimization affords the knowledge of such solutions and can help guide the decision maker by revealing where objectives can be achieved simultaneously and where they conflict. Having access to the set of Pareto efficient solutions may also help the decision maker locate solutions where compromises in one objective allow outweighing improvements in another. For instance the forest manager may discover that forgoing small amounts of timber revenues allows for the sequestration of significantly more carbon. Or the hospital may be able to increase patient throughput substantially if they hire one additional oncologist. Regardless of whether a decision maker selects a solution providing such gains, the awareness of these relationships enables more informed decision making.

In addition to studying conflict within a system, we may further study it at the super-system level. Consider the situation in which a decision maker oversees multiple systems, each with its own set of Pareto efficient solutions. This could be the case for a manager overseeing multiple hospitals or multiple food processing facilities. Alternatively, each system may correspond to a different regulatory or environmental scenario, such as a forest manager analyzing resource allocation under various realizations of climate change. In such instances, understanding the differences in the conflict relationships between systems may benefit the decision maker, allowing them to ask questions such as: How does the relationship between carbon sequestration and timber revenues vary under different climate change scenarios? Do all hospitals require the same increase in staffing costs to improve patient throughput?

To date, the multi-objective optimization literature has not addressed conflict at the super-system level. We do so for the first time here, laying a foundation for quantitative conflict analysis. To perform this investigation, we draw on Pareto set indicators and correlation measures commonly used in the field of evolutionary multi-objective optimization (EMO). In EMO, the Pareto set indicators are generally used to assess the performance of algorithms that approximate the Pareto set [28], and the correlation measures are used as

an aid to increase the computational tractability of the problems encountered in EMO [3].

Here we adapt these measures for real-world application, using them to study conflicting management objectives across systems. To further our insight into the origin of conflict within a system, we also propose a new metric for quantifying the conflict between pairs of objectives. The new pairwise conflict metric developed here improves on other commonly used pairwise conflict metrics such as the Pearson and Spearman coefficients. Unlike any current metric, the one we propose simultaneously captures mutual objective achievement and accurately identifies the absence of conflict between objectives. We demonstrate the novel utility of the existing and proposed conflict metrics on a multi-objective scenario-based case study in the Deschutes National Forest.

Our results show that our proposed process and new conflict metric are successful at quantifying and differentiating the amount of conflict within and across multi-objective systems and provide a useful tool for multi-objective decision making.

In the upcoming sections, we define terminology and the measures of conflict. Then we describe the case study and present its results, including the application of the new and existing conflict metrics. We conclude with a discussion, summary, and suggestions for future research.

1.2 Methods

We lay a foundation for quantitative conflict analysis of multi-objective systems. The analysis centers on the use of three metrics: two existing measures from EMO and one that we have developed and introduce for the first time here. A case study on the impacts of climate change on forest management serves to illustrate the conflict analysis. Prior to describing the case study, we first define terminology and describe each of the measures used in our analysis.

1.2.1 Terminology

The multi-objective problem Consider the M-objective optimization problem

Maximize

$$\mathbf{f} = [f_1(\mathbf{x}), f_2(\mathbf{x}), \ldots, f_M(\mathbf{x})] \tag{1.1}$$

subject to

$$\mathbf{x} \in X \tag{1.2}$$

with *objective functions* $f_i(\mathbf{x}), i \in \{1, \ldots, M\}$ and feasible *decision vectors* (or *solutions*) $\mathbf{x} \in \mathbb{R}^n$ where n is the number of decision variables in the optimization problem. A set of equality and inequality constraints determine the *feasible decision space* X. Solutions in X are referenced by superscripts: $X = \{\mathbf{x}^1, \mathbf{x}^2, \ldots, \mathbf{x}^{|X|}\}$. Each objective function $f_i : \mathbb{R}^n \mapsto \mathbb{R}$ maps decision vectors to scalars in $\mathbb{R}$. The vector objective function $\mathbf{f} : X \mapsto \mathbb{R}^M$ maps the feasible decision space to the *objective space* $\mathbb{R}^M$. The set of all objective functions is the *objective set* $\mathcal{M} = \{f_1, \ldots, f_M\}$.

Dominance and frontiers A solution $\mathbf{x}^1$ is said to *dominate* another solution $\mathbf{x}^2$ ($\mathbf{x}^1 \succ \mathbf{x}^2$) if

$$\exists f_i \in \mathcal{M} : f_i(\mathbf{x}^1) > f_i(\mathbf{x}^2) \text{ and } \forall f_i \in \mathcal{M}\ f_i(\mathbf{x}^1) \geq f_i(\mathbf{x}^2) \tag{1.3}$$

A solution $\mathbf{x}^1 \in X$ is *non-dominated* if

$$\nexists \mathbf{x}^2 \in X : \mathbf{x}^2 \succ \mathbf{x}^1 \tag{1.4}$$

For a rational decision maker, all dominated solutions may be removed from the analysis, since for a dominated solution $\mathbf{x}^2$ there exists another solution $\mathbf{x}^1$ which is better: $\mathbf{x}^1$ achieves more in at least one objective than $\mathbf{x}^2$, and $\mathbf{x}^1$ does not achieve less in any objective than $\mathbf{x}^2$. Thus, the decision maker will always select a solution from the set of non-dominated decision vectors that solve the multi-objective problem (1.1) and (1.2). We refer to this set as the *Pareto-optimal set* $P = \{\mathbf{x} \in X | \nexists \mathbf{y} \in X : \mathbf{y} \succ \mathbf{x}\}$.

The *Pareto-optimal frontier*, the *efficient frontier* or, simply, the *frontier* Z is the corresponding set of M-dimensional *objective vectors* $\mathbf{z} = [f_1(\mathbf{x}), f_2(\mathbf{x}), \ldots, f_M(\mathbf{x})]$. That is,

$$Z = \{\mathbf{z} = [f_1(\mathbf{x}), \ldots, f_M(\mathbf{x})] \mid \mathbf{x} \in P\} \tag{1.5}$$

Objective vectors' components are referred to in subscripts:

$$\mathbf{z} = [z_1, z_2, \ldots, z_M] \tag{1.6}$$

Objective vectors provide the decision maker with knowledge of the objective achievement of a solution $\mathbf{x}$ – the ith component of an objective vector $\mathbf{z}$ represents the achievement in objective i by the corresponding decision vector $\mathbf{x}$.

Ideal and nadir objective vectors The *ideal objective vector* is defined as the vector

$$\mathbf{z}^{\text{ideal}} = \max_{\mathbf{x} \in X} \{f_i(\mathbf{x})\} \quad \forall i \in \mathcal{M}. \tag{1.7}$$

Analogously, define the nadir solution as the vector

$$\mathbf{z}^{\text{nadir}} = \min_{\mathbf{x} \in X} \{f_i(\mathbf{x})\} \quad \forall i \in \mathcal{M}. \tag{1.8}$$

The ideal objective vector represents the impossible ideal scenario in which each objective is simultaneously optimized. The nadir objective vector represents the worst case scenario in which each objective attains its lowest value. These solutions are the diagonal corners of the minimum bounding box for the efficient frontier Z. Since together they provide upper and lower bounds for each objective, they serve as reference points against which the decision maker can compare solutions.

Trade-offs The *trade-off* between two objective vectors $\mathbf{z}^1$ and $\mathbf{z}^2$ is the vector of differences in their objective achievements:

$$\tau^{1,2} = [z_1^2 - z_1^1, z_2^2 - z_2^1, \ldots, z_M^2 - z_M^1] \tag{1.9}$$

The components of $\tau^{1,2}$ represent the amount of each objective that would be sacrificed or gained if the decision maker selected solution $\mathbf{z}^2$ instead of $\mathbf{z}^1$. Note that $\tau^{1,2} = -\tau^{2,1}$.

Sub-dimensions During analysis, we often wish to consider only a subset of the objectives $\mathcal{L} \subset \mathcal{M}$. We define such subsets as *sub-dimensional objective sets*. In these cases, it is simpler to work with constructs that have only those components that correspond to the objectives in $\mathcal{L}$. For instance, define the *sub-dimensional objective vector* for the solution $\mathbf{x}^i$ as $\mathbf{z}^i_{\mathcal{L}}$ which has components $\forall \ell \in \mathcal{L}\ z^i_\ell = f_\ell(\mathbf{x}^i)$. Define the *sub-dimensional trade-off* $\tau^{1,2}_{\mathcal{L}}$ as the vector with components $\forall \ell \in \mathcal{L}\ \tau^{1,2}_\ell$.

Relative objective achievements, relative objective vectors, and relative trade-offs Using the nadir and ideal objective vectors, we can represent each solution as a vector of its relative objective achievements, each taking a value in $[0, 1]$. This allows for dimensionless and scale-agnostic comparison of solutions. For an objective vector $\mathbf{z}$, its *relative achievement in objective* i is

$$\overline{z_i} = \frac{z_i - z_i^{\text{nadir}}}{z_i^{\text{ideal}} - z_i^{\text{nadir}}}, \tag{1.10}$$

and the corresponding *relative objective vector* is

$$\bar{\mathbf{z}} = [\overline{z_1}, \overline{z_2}, \ldots, \overline{z_M}]. \tag{1.11}$$

For two objective vectors $\mathbf{z}^1$ and $\mathbf{z}^2$, the corresponding *relative trade-off* is

$$\bar{\tau}^{1,2} = \left[\overline{z_1^2} - \overline{z_1^1}, \overline{z_2^2} - \overline{z_2^1}, \ldots, \overline{z_M^2} - \overline{z_M^1}\right] \tag{1.12}$$

Conflict, monotonicity, bundles and stacks Objectives in an objective set $\mathcal{L}$ *do not conflict* if the objectives improve simultaneously: $\forall \mathbf{z}^1, \mathbf{z}^2 \in Z,\ i, j \in \mathcal{L},\ j \neq i$

$$(z_i^1 \geq z_i^2) \Rightarrow (z_j^1 \geq z_j^2) \tag{1.13}$$

If (1.13) does not hold, then the objectives conflict. Any pair of objectives $i, j \in \mathcal{M}$ such that equation (1.13) holds are said to *increase monotonically*. In the case of monotonically increasing objectives i and j, improving objective i also yields improvement in objective j. Conversely, if

$$(z_i^1 \geq z_i^2) \Rightarrow (z_j^1 \leq z_j^2) \quad \forall \mathbf{z}^1, \mathbf{z}^2 \in Z, j \neq i \tag{1.14}$$

holds, then objectives i and j are said to *decrease monotonically*.

When the objectives represent goods or services, a set of objectives that conflict is defined as a *bundle* and a set of objectives that do not conflict is defined as a *stack*.

Equation (1.13) checks for monotonically increasing relationships among objectives. This means of detecting conflict is functionally equivalent to that used by many past studies, such as Brockhoff and Zitzler (2009) [4] and Purshouse and Fleming (2003) [19].

1.2.2 Measuring conflict: the hypervolume indicators

Any multi-objective problem whose efficient frontier consists of more than one solution contains conflict. The decision maker responsible for these multi-objective systems must determine which solution represents the best compromise among the objectives, and understanding the conflict in the system imroves their ability to do so. This includes both the amount of system conflict as well as the source of that conflict. For the former, we can draw on existing measures from EMO; for the latter, we propose a new metric that quantifies the conflict between pairs of objectives. We begin with a description of the measures from EMO that we use to measure system-level conflict: the hypervolume indicators.

Hypervolume indicator

The *hypervolume indicator* $I_{H1}(Z)$ measures the percentage of the objective space that is bounded by the non-dominated objective vectors $\mathbf{z} \in Z$. See Figure 1.1. Systems with less conflict will produce solutions with greater joint provision of objectives, leading to a greater proportion of enclosed objective space and thus a larger value for the hypervolume. In contrast, systems with more conflict produce solutions with less joint provision of objectives, leading to a lesser proportion of enclosed objective space and a smaller value for the hypervolume. That is, the greater the value of the hypervolume indicator, the lower the conflict in the system.

To measure the hypervolume indicator, for each relative objective vector $\overline{\mathbf{z}}^i$ in the frontier Z, define its corresponding hyperrectangle r_i. r_i is the M-orthotope with opposite corners

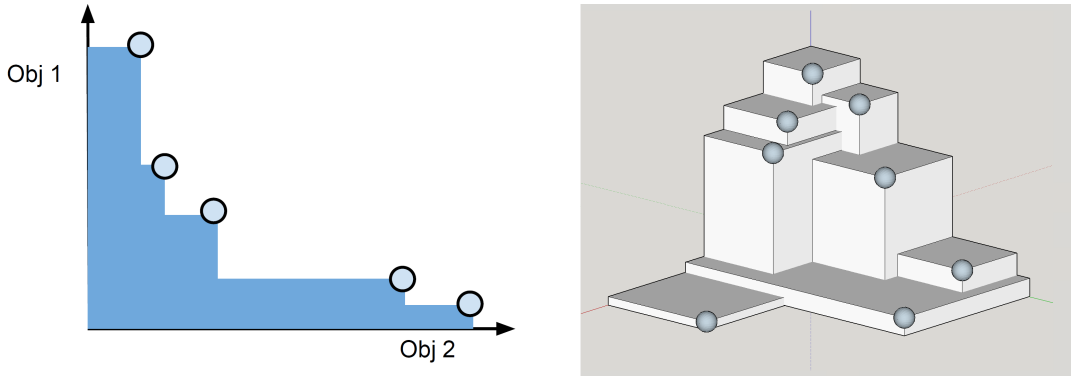

Figure 1.1: Depiction of the hypervolumes of frontiers with two objectives (left) and three objectives (right).

the origin and the point defined by the components of the relative objective vector $\overline{\mathbf{z}}^i$. Then the hypervolume indicator is the volume of the union of these hyperrectangles:

$$I_{H1}(Z) = \text{vol}\left(\bigcup_{i=1}^{|Z|} r_i\right). \tag{1.15}$$

Given two frontiers Z^1 and Z^2, how do you interpret a difference in their hypervolumes? Consider Figure 1.2 which shows the relative objective space for a two-dimensional frontier. The shaded square in the lower left represents an achievement of 10% in each objective. Since the objective space of the relative objective vectors is bounded by the 1×1 square, this corresponds to 1% of the objective space. So if Z^1 and Z^2 are bi-objective frontiers ($M = 2$) and if $I_{H1}(Z^1) - I_{H1}(Z^2) = 0.01$, then the solutions in frontier Z^1 bound an area equivalent to an additional 10% achievement in each objective beyond that bounded by the solutions in Z^2. Small differences in the values of the hypervolume represent significant objective gains.

In general, an increase of h in the value of the hypervolume equates to an increase in each objective of $h^{1/M}$. So if Z^1 and Z^2 were tri-objective ($M = 3$) then an improvement of .01 in the value of the hypervolume would represent an improvement of about 22% in each objective.

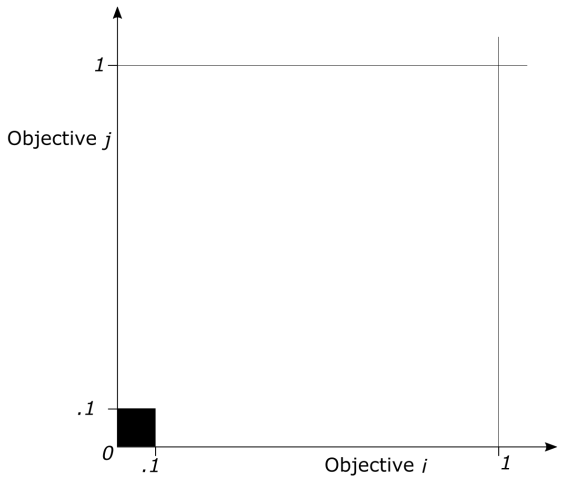

Figure 1.2: To compute the hypervolume, we use the relative objective vectors for the solutions in a frontier. Thus, the frontier is bounded by the M-cube which has a pair of diagonal corners at the origin and $\vec{1}$. Shown here is the 2-cube (a square) representing the space in which we compute the hypervolume for a bi-objective frontier ($M = 2$). The space bound by the shaded square in the lower left represents an achievement of 10% in each objective yet makes up only 1% of the objective space. Its intent is to show that small differences in hypervolumes are significant: with two objectives, an improvement of 0.01 in the value of the hypervolume represents an additional achievement of 10% in each objective.

Binary Hypervolume Indicator

If a frontier Z^2 is found to have a smaller hypervolume than another Z^1, one may wonder whether Z^2 is completely enclosed within Z^1 or simply bounds a different but smaller region of the relative objective space. We use the binary hypervolume indicator to address this question. The binary hypervolume $I_{H2}(Z^1, Z^2)$ computes the volume of the objective space bounded by Z^1 but not by Z^2. See Figure 1.3. As such, if Z^2 is completely enclosed within Z^1, then $I_{H2}(Z^2, Z^1) \leq 0$. On the other hand, if $I_{H2}(Z^2, Z^1) > 0$ then Z^2 encloses regions of the objective space that Z^1 does not.

Following the definition proposed by Zitzler (1999) [27], the *binary hypervolume indicator* of two frontiers Z^1 and Z^2 is [27]

$$I_{H2}(Z^1, Z^2) = I_{H1}(Z^1 + Z^2) - I_{H1}(Z^2) \tag{1.16}$$

where $I_{H1}(Z^1 + Z^2)$ is the hypervolume indicator of the frontier that consists of the non-dominated points in $\{Z^1 \cup Z^2\}$. See the lower-left panel in Figure 1.3.

1.2.3 Computing the hypervolume indicator

Computing the hypervolume is a nontrivial task that has received attention from the EMO community. For a comparison of previous algorithms that compute the hypervolume, see While (2006) [26]. We developed our own algorithm to compute the hypervolume indicator.

The algorithm begins with a list of the relative objective vectors (in describing the algorithm here, we omit the bar and simply denote them by $\mathbf{z} \in Z$). These vectors are assumed to be sorted in descending order based on their mth component, for some arbitrary objective $m \in \mathcal{M}$. We define the sub-dimensional objective set $\mathcal{L} = \mathcal{M} \backslash \{m\}$ whose cardinality we denote by $|\mathcal{L}| = L = M - 1$.

We initialize the algorithm with an empty set G of non-dominated solutions in L dimensions. Let the volume of this set be denoted $\overline{V}$. We add solutions $\mathbf{z}$ from Z to G in order of decreasing z_m, at each iteration adding the contribution of the solution $\mathbf{z}$ to the hypervolume indicator V. These contributions are computed by multiplying the solution's

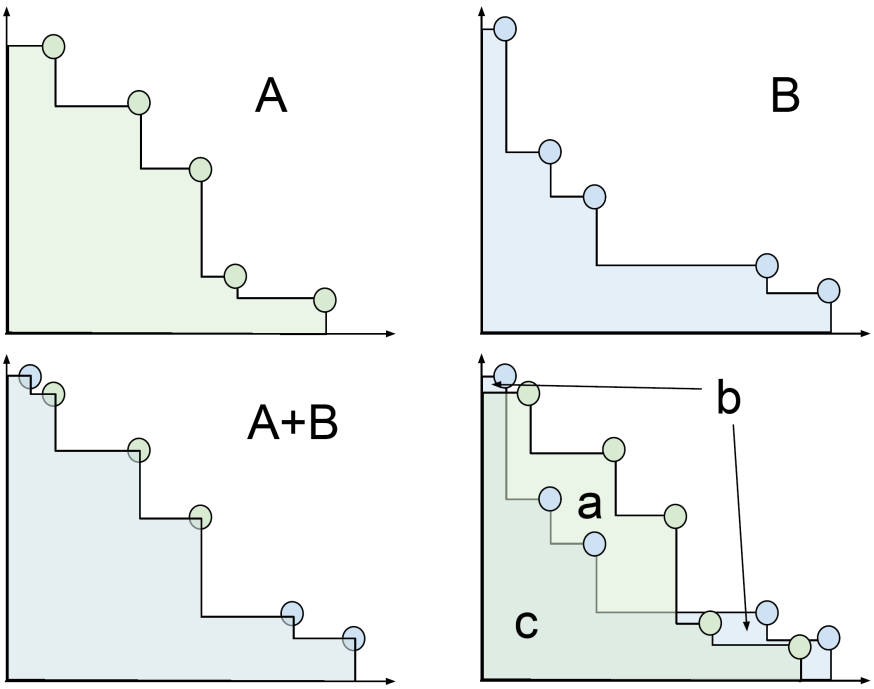

Figure 1.3: Depiction of the binary hypervolume indicator. The individual frontiers are shown in the top row: frontier A (left) and frontier B (right). The merged frontier $A + B$ is shown in bottom left - note the absence of points that were dominated when combined. Following the naming of regions as shown in the bottom right figure, the binary hypervolume indicator is equal to

$$I_{H2}(A, B) = (\text{area}_a + \text{area}_b + \text{area}_c) - (\text{area}_b + \text{area}_c) = \text{area}_a$$

mth component z_m by $\overline{V}_{\mathbf{z}}$, its contribution to the volume of G. See Figure 1.5 for a visual reference (the solutions' contribution to the volume of G, $\overline{V}_{\mathbf{z}}$, are the yellow regions in the figure).

We compute $\overline{V}_{\mathbf{z}}$ as follows. Initialize $\overline{V}_{\mathbf{z}} = 0$, and add $\mathbf{z}$ to the set G. Remove from G any solutions that are dominated by $\mathbf{z}$ in L dimensions. Add to $\overline{V}_{\mathbf{z}}$ the value of the volume of $\mathbf{z}$ in L dimensions (the union of the yellow and gray areas in Figure 1.5); this is simply the product of its components z_ℓ for $\ell \in \mathcal{L}$. Then subtract from $\overline{V}_{\mathbf{z}}$ the volume of G prior to the addition of $\mathbf{z}$ (the union of the gray and white areas in Figure 1.5). The last step is to compute and add back in the volume of the "sides" of G that were subtracted in the

previous step (the white areas in Figure 1.5). This "sides" volume is computed by taking the sum over each dimension $\ell \in \mathcal{L}$ of the areas along that dimension enclosed by the existing solutions in G. Pseudocode for this algorithm is presented in Figure 1.4.

Figure 1.4: Algorithm to compute the hypervolume V of a Pareto frontier. Prior to running the algorithm, pick an objective m from the objective set $\mathcal{M}$ and define the sub-dimensional objective set $\mathcal{L} = \mathcal{M} \backslash \{m\}$. Then sort $\mathbf{z} \in Z$ in descending order by their mth component. Here, $\mathbf{z} \in Z$ is the set of relative objective vectors. Let $\overline{V}_{\mathbf{z}}$ be the $(M-1)$-dimensional volume contribution of the solution $\mathbf{z}$, and let $\mathbf{g} \in G$ be the non-dominated objective vectors in $M-1$ dimensions.

$V \leftarrow 0$
$\overline{V} \leftarrow 0$
$G \leftarrow \emptyset$
for all $\mathbf{z} \in Z$ **do**
    $\overline{V}_{\mathbf{z}} \leftarrow \prod_{\ell \in \mathcal{L}} z_\ell - \overline{V}$
    for all $\mathbf{g} \in G$ **do**
        if $\forall \ell \in \mathcal{L}\ g_\ell < z_\ell$ **then**
            $G \leftarrow G \backslash \{\mathbf{g}\}$
        end if
    end for
    for all $\ell \in \mathcal{L}$ **do**
        $G_{\mathbf{z},\ell} := \{\, \mathbf{g} \in G : g_\ell > z_\ell \,\}$
        Sort $\mathbf{g} \in G_{\mathbf{z},\ell}$ in ascending order by ℓth component, g_ℓ
        $v_i \leftarrow z_\ell$
        for all $\mathbf{g} \in G_{\mathbf{z},\ell}$ **do**
            $v_t \leftarrow g_\ell$
            $\delta_\ell := v_t - v_i$
            $\overline{V}_{\mathbf{z}} \leftarrow \overline{V}_{\mathbf{z}} + \delta_\ell \prod_{\lambda \in \mathcal{L} \backslash \{\ell\}} g_\lambda$
            $v_i \leftarrow v_t$
        end for
    end for
    $G \leftarrow G \cup \{\mathbf{z}\}$
    $\overline{V} \leftarrow \overline{V} + \overline{V}_{\mathbf{z}}$
    $V \leftarrow V + z_m \overline{V}_{\mathbf{z}}$
end for

Figure 1.5: **Computing the hypervolume of a 3D frontier: first three iterations of the algorithm** (process moves from left to right). Consider a three-dimensional frontier Z. We sequentially add solutions to a 2D projection of the frontier, seen here. The solutions are added in order of decreasing value in their third component (height – not seen here). At each iteration, we compute the contribution in 2D as follows: Add the product of the solution's 2D components (the union of the yellow and gray areas). Then subtract all the previous existing 2D frontier area (the union of the gray and white areas). Then add back the value of the sides (white areas). This yields the value of the yellow area. Multiply this value by the third component of the solution to obtain the solution's contribution to the hypervolume V.

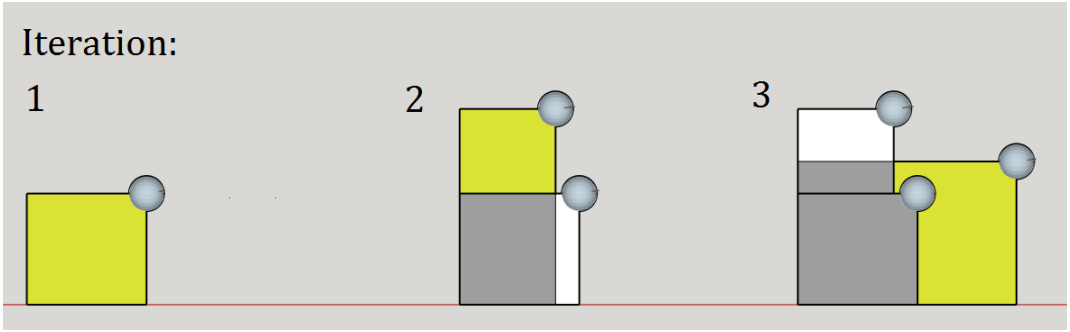

1.2.4 A new measure for pairwise objective conflict

When the hypervolume indicates that there is conflict in the system, how does the decision maker determine which objectives are responsible for the conflict? In the case of the hospital, is it cost and patient throughput that are most conflicting, or is it cost and required back-up? For the forest manager, are carbon sequestration and timber revenue the incompatible objectives responsible for the low hypervolume value, or is it wildlife habitat and timber revenue? If the forest manager oversees multiple independent forests, they may also ask whether the answers to these questions are the same in each. With the suite of measures currently available, the decision maker cannot adequately answer these questions. Here we propose a new measure of conflict to fill this void.

To motivate the metric, we consider the simple example in Figure 1.6. For the frontiers shown here, the conflict between objectives i and j is greatest in Frontier C and least in

Frontier A (all objectives are maximized).

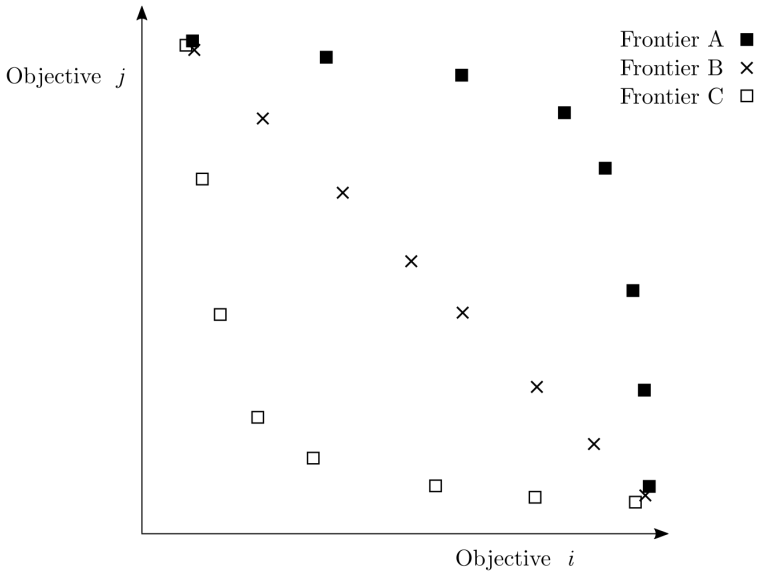

Figure 1.6: Varying conflict between objectives. The conflict between maximization objectives i and j increases from Frontier A to Frontier B to Frontier C.

Many authors have previously measured conflict between objectives [4][19][11], with most commonly used metrics deriving from measures of linear correlation (such as the Pearson correlation coefficient [9]) or rank correlation (such as Kendall's Tau [16] or Spearman's rho [17]). The motivation behind these metrics is often the removal of redundant objectives from a many-objective optimization problem. In such cases, these measures of monotonicity or correlation alone suffice. However, they fall short of providing a quantification of conflict between pairs of objectives for the sake of decision making or more general system analysis. For instance, metrics for linear correlation are limited in their ability to capture the montonicity between objectives, which is the fundamental principle that determines if objectives conflict. Furthermore, both linear and rank correlation metrics fail to capture the objective achievement of the solutions. Thus, for a more nuanced understanding of the relationship between the objectives, a different metric is required.

Let $\mathbf{z}_{ij}$ be the sub-dimensional objective vector comprised of only the components cor-

responding to the ith and jth objectives $\mathbf{z}_{ij} = [z_i, z_j]$. We define the following measure of conflict between objectives i and j:

$$C_{ij} = \frac{(1 - \rho_{ij})\bar{d}_{ij}}{2d_{\max,ij}} \tag{1.17}$$

where $\bar{d}_{ij}$ is the average sub-dimensional distance from objective vectors to the ideal solution:

$$\bar{d}_{ij} = \frac{1}{|Z|} \sum_{\mathbf{z} \in Z} ||\mathbf{z}_{ij}^{\text{ideal}} - \mathbf{z}_{ij}|| \tag{1.18}$$

and

$$d_{\max,ij} = ||\mathbf{z}_{ij}^{\text{ideal}} - \mathbf{z}_{ij}^{\text{nadir}}|| \tag{1.19}$$

and ρ_{ij} is Spearman's rank-correlation coefficient for the solutions' achievements in objectives i and j. Note that $C_{ij} \in [0, 1)$, taking smaller values when there is less conflict between objectives i and j and larger values when there is more.

The conflict metric proposed here (equation (1.17)) addresses two major issues:

1. **Indifference to non-conflicting relationships**. Per equation (1.13), when an objective i increases monotonically with another objective j, the objectives do not conflict. Accordingly, C_{ij} should equal 0 in all such cases. This is true for the new metric, since for monotonically increasing objectives $\rho_{ij} = 1$, so $1 - \rho_{ij} = 0$.

2. **Consideration of objective achievement**. Recall Figure 1.6 and the intuitive notion that the conflict between objectives i and j is stronger in Frontier C than it is in Frontier B than it is in Frontier A. This notion is guided by the idea that the closer objective vectors are to the sub-dimensional ideal solution on average, the less the conflict between the objectives; that is, that greater simultaneous objective provision is indicative of less conflict. The proposed metric accounts for this, while correlation measures do not. In the extreme case of monotonically decreasing objectives, $\frac{(1-\rho_{ij})}{2} = 1$, so $C_{ij} = \frac{\bar{d}ij}{d_{\max,ij}}$. See Figure 1.7 for an example.

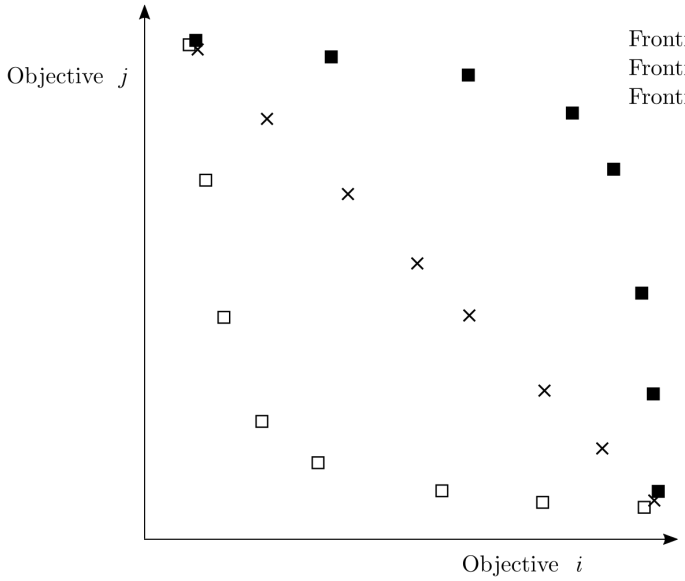

	Proposed C_{ij}	Pearson ρ_{ij}	Spearman $\rho_{s,ij}$
Frontier A	*0.4*	*-0.6*	*-1*
Frontier B	*0.6*	*-1*	*-1*
Frontier C	*0.8*	*-0.6*	*-1*

Figure 1.7: Comparing the proposed metric for conflict C_{ij} against the Pearson product-moment and the Spearman rank correlation coefficients (ρ_{ij} and $\rho_{s,ij}$, respectively). While the latter two are identical for frontiers A and C, the proposed metric is greater for frontier C than it is for A. This is because it accounts for the average relative distance to the sub-dimensional ideal objective vector.

To interpret differences in C_{ij} for different objective pairs, we may decompose the metric into components: one for rank correlation

$$c_{ij,\rho} = \frac{1 - \rho_{ij}}{2}, \tag{1.20}$$

and one for objective achievement

$$c_{ij,d} = \frac{\bar{d}ij}{d_{\max,ij}}. \tag{1.21}$$

The comparison of these components for different objective pairs can be used to infer whether the solutions primarily vary in their joint provision of objectives or in their general ordering. For large enough frontiers, a significance test is available for ρ_{ij} to determine whether it is significantly different from 0 (if $c_{ij,\rho}$ is significantly different from 0.5).

1.3 Case Study

To demonstrate the application of the hypervolume indicators and the proposed pairwise objective metric to the analysis of conflict in multi-objective systems, we perform a case study on forest management in the Deschutes National Forest. We compare the conflict among ecosystem services in three multi-objective systems: one in which climate change is ignored, one in which climate change is predicted to be mild, and one in which it is predicted to be severe. For each climate change scenario, we solve a multi-objective mathematical program that optimizes ecosystem service achievement. The model aims to minimize fire hazard and sediment delivery while maximizing habitat for the northern spotted owl. In the coming sections we describe the study area and the importance of each of these ecosystem services. We then formally define the mathematical program solved for each climate change scenario, describe the climate scenarios considered, and finally present and discuss the results.

1.3.1 Study area and selection of ecosystem services

Our study area is the Drink Planning Area. It consists of 7056 ha of federally owned forest land on the east slopes of the Cascade Mountain Range located within the Deschutes National Forest. See Figure 1.8. Having never undergone logging or treatment, the Drink contains large areas of old growth forest. The large swaths of old growth forest in the Drink make it prime habitat for the northern spotted owl (NSO) (*Strix occidentalis caurina*, Figure 1.9), an iconic inhabitant of Pacific Northwest forests that is listed as a federally threatened species [5]. However, the same old growth conditions that render the area suitable habitat for the NSO also render it susceptible to high-severity wildfires. Such a wildfire would put at risk the NSO's habitat [6] as well as one of the Drink's other notable features - the municipal watershed for the cities of Bend, OR and Sisters, OR. Wildfires pose a threat to these cities' water supply, because they can cause soil water repellency, surface runoff, and debris torrents [14] which degrade watershed quality.

For these reasons, the managing entity, the United States Forest Service (USFS), would

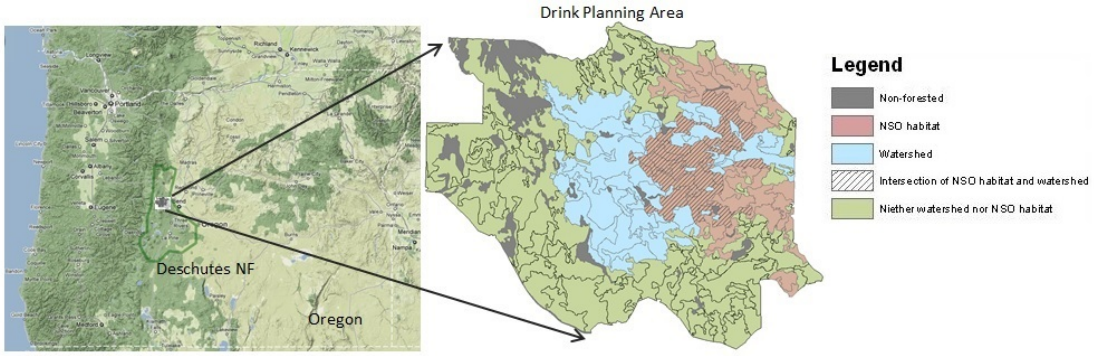

Figure 1.8: Overview of the study system, the Drink Planning Area, consisting of 7056 ha in the Deschutes National Forest. The Drink Area contains old growth forest that make it suitable habitat for the northern spotted owl. It also houses the municipal watershed for Bend, OR and Sisters, OR.

like to perform fuel removals in the Drink in order to reduce the area's fire hazard. However, performing these fuel removals has the potential to disrupt the habitat of the NSO [2] and to induce short-term increases in sediment delivery [18]. The latter is expected to be especially true in the Drink Area, where local USFS staff have noted that the watershed is unusually susceptible to spikes in sediment delivery as a result of foot traffic and other activities that occur within the watershed.

We developed a multi-objective mathematical program that optimizes the joint provision of these conflicting ecosystem services[1].

1.3.2 The multi-objective model

The multi-objective model is a zero-one mathematical program that assigns spatiotemporal prescriptions for fuel removals across the Drink Area to optimize the joint provision of

[1]These represent only a subset of the ecosystem services of concern to the USFS in the Drink Area. While the USFS manages for many ecosystem services simultaneously, many of the services are stacked rather than bundled, meaning the ecosystem services are not in conflict. These services need not all be considered in the multi-objective model, because the selection and maximization of one ecosystem service entails the maximization of all in the stack. For this reason, we have disregarded non-conflicting ecosystem services and selected a minimal bundle on which to employ multi-objective optimization. Those that do not conflict can be stacked post-optimization.

Figure 1.9: The northern spotted owl is a threatened species whose habitat includes forests in the Pacific Northwest, including the Drink Area.

ecosystem services. Spatially, the model prescribes fuel removals across 303 forest stands into which the Drink has been divided (the interior polygons in Figure 1.8). Temporally, the model operates over an 80-year planning horizon, from 2015 to 2095. The fuel removals are scheduled in two 20-year treatment periods: 2015-2035 and 2035-2055. For each stand, the model may prescribe fuel removals in the first period, the second period, neither, or both.

To ensure long-term efficacy of the fuel removals, the model minimizes the fire hazard rating of the Drink Area at the end of the 80-year planning horizon. To mitigate impacts of the fuel removals on NSO habitat, the model maximizes the area of NSO habitat at the end of each planning period. Similarly, the model minimizes the short-term spikes in sediment delivery resulting from the application of fuel removals, which are assumed to be performed at the midpoint year in the treatment periods (years 2025 and 2045). Figure 1.10 contains a schematic of the planning horizon which shows the timing of these events.

Notation

We use the following notation in the development of the model:

Model parameters

- $i \in I$**:** the set of forest stands comprising the Drink Area ($|I| = 303$)

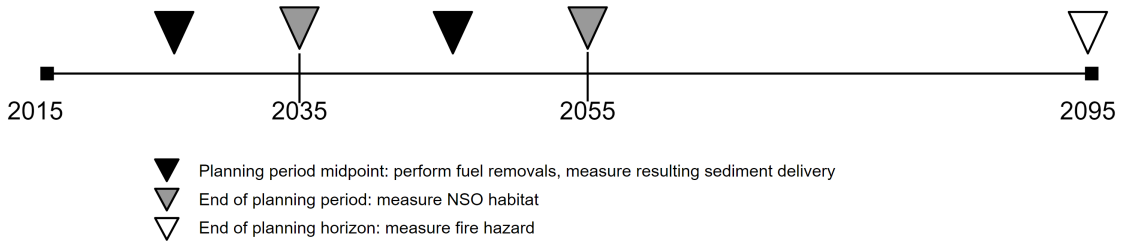

Figure 1.10: The planning horizon used in the case study spans the 80 year period from 2015 to 2095. Fuel removals may be performed in the first period (2015-2035), the second period (2035-2055), both, or neither. Fuel removals are assumed to be performed at the mid-point years of each period (black triangles). Sediment delivery is measured on treatment years. Stands' suitability for NSO habitat is measured at the end of the planning periods (gray triangles), and stands' fire hazard ratings are measured at the end of the planning horizon (white triangle).

- a_i**:** the area of stand i

- $r \in R$**:** the set of fuel removal prescriptions:

$$r = \begin{cases} 1 & \text{fuel removals in the first period (2015-2035)} \\ 2 & \text{fuel removals in the second period (2035-2055)} \\ 3 & \text{fuel removals in both periods} \\ 0 & \text{no fuel removals performed in either period} \end{cases}$$

- $F_{i,r}$**:** the area-weighted fire hazard rating of stand i at the end of the planning horizon if prescribed to fuel removal schedule r. The metric for fire hazard rating used in this analysis originated in the work by Schroder *et al.* [20]. This metric was developed for the Drink Area. It uses fire characteristics from the set of fuel models proposed by Anderson [1] in order to assign a fire hazard rating. I expanded the rating system to include fuel models not present in Schroder *et al.* See Table 1.1 for the mapping of fuel models to fire hazard ratings.

  The USFS's Climate-Forest Vegetation Simulator (Climate-FVS) was used to generate

the fuels and vegetation characteristics of the stands in order to determine their fire hazard rating. Initial vegetation data for Climate-FVS came from the 2012 GNN structure map (`http://lemma.forestry.oregonstate.edu/data/structure-maps`) from Oregon State University's Landscape Ecology, Modeling, Mapping & Analysis (LEMMA) group. Plots from the LEMMA database were mapped to the stands in the Drink area in order to produce tree and stand lists. These lists were used with Climate-FVS to simulate the stands' vegetation and fuels characteristics forward for the duration of the planning horizon under each climate scenario. Input climate data for Climate-FVS was obtained through the Climate-FVS climate data server [8].

Fuel Model	**Fire Hazard Rating**	Group	Flame length (m)	Rate of spread (m/hr)	Total fuel load (tons/ha)
4*	**5**	Shrub	5.79	1508.76	32.12
5	**4**	Shrub	1.22	362.10	8.65
8	**1**	Timber	0.30	32.19	12.36
9*	**2**	Timber	0.79	150.88	8.65
10	**2**	Timber	1.46	158.92	29.65
11*	**2**	Logging Slash	1.07	120.7	28.42
12	**4**	Logging Slash	2.44	261.52	85.50
13	**5**	Logging Slash	3.20	271.58	143.57

Table 1.1: Fire hazard rating system used here, originally employed by Schroder *et al.* [20]. Asterisks (*) denote fuel models not present in Schroder *et al.*
The fuel model column refers to the Anderson fuel model ratings [1].

- $I_{\omega,t}$**:** the set of stands that qualify as NSO habitat at the end of planning period t under at least one fuel removal schedule. The stands that qualify as NSO habitat at the end of a planning period t are those that meet the following three criteria in year t, as specified by the USFS:

  1. elevation less than 1830 m
  2. the presence of trees with diameter at breast height (DBH) at least 76 cm
  3. canopy closure of at least 60%

The elevation requirement was checked using a digital elevation model from the US Department of Agriculture's GeoSpatial Data Gateway; canopy closure and large tree criteria were determined using the simulated vegetation characteristics output from Climate-FVS.

In addition, to account for the large habitat requirements of the NSO, stands must be members of a cluster exceeding 200 ha in size, the entirety of which meets the aforementioned NSO habitat criteria. Stands that meet the first three criteria but are not part of such a cluster are less valuable NSO habitat and therefore have their contributions to the total owl habitat discounted by a factor of e.

- e**:** the discount factor applied to NSO habitat when it is not part of a contiguous habitat cluster at least 200 ha in size. Following the convention used in Schroder *et al.* [20], we set $e = 0.5$.

- $j \in R_{i,t}$**:** the set of fuel removal schedules such that stand i qualifies as NSO habitat at the end of planning period t. For instance, consider stand $i = 15$ and planning period $t = 2$ (2035-2055). We seek to find the set of fuel removal prescriptions $r \in R$ such that stand 15 is suitable NSO habitat at the end of planning period 2 (in year 2055). We enumerate the vegetation characteristics of stand 15 for all possible fuel removal schedules and determine that if fuel removals are assigned in the second planning period, then stand 15 does not qualify as NSO habitat in year 2055. Thus, $R_{15,2} = \{0, 1\}$, since for $r = 0$ (no fuel removals performed) and $r = 1$ (fuel removals performed in first period only), stand 15 does qualify as NSO habitat in 2055.

- $s_{i,t}$**:** the amount of sediment (in tonnes) delivered to the watershed as a result of performing fuel removals on stand i in planning period t. The contributions of sediment delivery from treatment of stand i in period t were determined using the online GIS tool for the Watershed Erosion Prediction Project (WEPP) [10]. This tool takes soil textures, treatment types, duration of simulation, and custom climate data as inputs.

Soil texture data for the Drink area was obtained from the USDA's Soil Survey Geographic (SSURGO) database, treatment types are those specified in §A, and the years of simulation correspond to the treatment years in the planning horizon (2015-2095). The custom climate data are those described above for use with Climate-FVS, obtained through the Climate-FVS data server.

- $c \in C$**:** Recall that the quantification of NSO habitat depends on the availability of large contiguous habitat patches; areas of NSO habitat less than than 200 ha in size are discounted. In order to determine when habitat is provided in sufficiently large areas, we must enumerate the set of clusters of stands whose combined area exceeds 200 ha. This set of clusters is the set C.

- $i \in D_c$**:** Given a cluster $c \in C$, the set D_c is the set of stands that comprise cluster c.

- $c \in C_i$**:** Given a stand i, we define the set C_i as the set of clusters that contain stand i

- A**:** the maximum area in hectares that may be treated in either planning period. We constrain the allowable treatment area per period to account for the limited availability of work crews to perform the fuel removals. Following guidance from the USFS, we set $A = 2428$ ha (approximately 6000 ac).

- ℓ**,** u**:** the lower and upper bounds, respectively, on the relative fluctuation in the area treated in periods 1 and 2. These bounds are used to enforce regulation in the workflow for the USFS. Here we use values such that the area for which fuel removals are performed does not fluctuate more than 20% between treatment periods; that is, we set the lower bound $\ell = 0.8$ and the upper bound $u = 1.2$.

Decision Variables

$$x_{i,r} = \begin{cases} 1 & \text{if stand } i \text{ is prescribed to treatment schedule } r \\ 0 & \text{otherwise} \end{cases}$$

Indicator Variables

- $q_{c,t} = 1$ if all stands in cluster c qualify as NSO habitat at the end of planning period t; $q_{c,t} = 0$ otherwise

- $p_{i,t} = 1$ if in planning period t stand i is part of a cluster c such that $q_{c,t} = 1$; $p_{i,t} = 0$ otherwise

Accounting Variables

- S_t**:** the total sediment delivered to the watershed from performing fuel treatments in planning period t

- O_t**:** the amount of NSO habitat (in hectares) at the end of planning period t

- H_t**:** the total area (in hectares) treated in planning period t

Model formulation

The formulation of the multi-objective model is as follows:

$$Minimize$$

$$\sum_{i \in I} \sum_{r \in R} F_{i,r} x_{i,r} \tag{1.22}$$

$$\max\{S_1, S_2\} \tag{1.23}$$

$$Maximize$$

$$\min\{O_1, O_2\} \tag{1.24}$$

Subject to:

$$\sum_{i \in I_{\omega,t}} \left(a_i p_{i,t} + e a_i \left(\sum_{j \in R_{i,t}} x_{i,j} - p_{i,t} \right) \right) = O_t \qquad \forall t \in \{1,2\} \tag{1.25}$$

$$\sum_{i \in I} \sum_{r \in 1,3} s_{i,1} x_{i,r} = S_1 \tag{1.26}$$

$$\sum_{i \in I} \sum_{r \in 2,3} s_{i,2} x_{i,r} = S_2 \tag{1.27}$$

$$\sum_{i \in D_c} \sum_{j \in R_{i,t}} x_{i,j} - |c| q_{c,t} \geq 0 \qquad \forall t \in \{1,2\}, c \in C \tag{1.28}$$

$$\sum_{c \in C_i} q_{c,t} - p_{i,t} \geq 0 \qquad \forall t \in \{1,2\}, i \in I_{\omega,t} \tag{1.29}$$

$$\sum_{r \in R} x_{i,r} = 1 \qquad \forall i \in I \tag{1.30}$$

$$\sum_{i \in I} \sum_{r \in 1,3} a_i x_{i,r} = H_1 \tag{1.31}$$

$$\sum_{i \in I} \sum_{r \in 2,3} a_i x_{i,r} = H_2 \tag{1.32}$$

$$H_t \leq A \qquad \forall t \in \{1,2\} \tag{1.33}$$

$$\ell H_1 - H_2 \leq 0 \tag{1.34}$$

$$-u H_1 + H_2 \leq 0 \tag{1.35}$$

$$x_{i,r}, p_i, q_c \in \{0,1\} \quad \forall i \in I, r \in R, c \in C \tag{1.36}$$

Equations (1.22)-(1.24) are the objective functions: equation (1.22) minimizes the cumulative fire hazard rating of the Drink Area at the end of the 80-year planning horizon, equation (1.23) minimizes the maximum peak in sediment delivery for the two planning periods, and equation (1.24) maximizes the minimum NSO habitat available at the end of the planning periods. Equation set (1.25) defines the amount of NSO habitat available at the end of the planning horizons. Note that if stand i does not belong to a cluster of NSO habitat exceeding 200 hectares, then its area contribution to total NSO habitat is discounted by a factor of e. Equations (1.26) and (1.27) define the sediment delivered in planning periods

one and two, respectively.

Inequality set (1.28) controls the value of the cluster variables $q_{c,t}$ indicating clusters that meet the NSO habitat criteria in each of the planning periods. Inequality set (1.29) controls the value of the $p_{i,t}$ variables indicating whether stand i is included in a cluster of NSO habitat at time t.

The set of equalities (1.30) enforces the logical constraint that each stand must be prescribed to exactly one fuel removal schedule. Equations (1.31) and (1.32) are accounting constraints for the total area treated in each planning period, and inequalities (1.33) ensure that this area does not exceed the predefined maximum. Inequalities (1.34) and (1.35) bound the fluctuation in treated area between the planning periods. Finally, constraint (1.36) defines the decision and indicator variables as binary.

1.3.3 Solution method

We developed an implementation of Tóth's Alpha-Delta algorithm [22] to solve the model (1.22)-(1.36) utilizing the IBM ILOG CPLEX optimization engine. For a problem with M objectives, the Alpha-Delta algorithm finds the Pareto frontier by iteratively slicing the M-dimensional objective space with a tilted $M-1$-dimensional hyperplane. The algorithm was implemented using an alpha parameter of $\alpha = .01$ and delta parameters of $\delta_{Hab} = 1$ ha and $\delta_{Sed} = 2$ tonnes for the NSO habitat and sediment delivery objectives, respectively.

1.3.4 Climate change scenarios

Like other ecosystems, forests will undergo changes as a result of the changing climate. For instance, researchers anticipate new spatial distributions of tree species [15], increased sediment delivery to streams [12], and increasing disturbance regimes such as wildfires, droughts, and insect infestations [24]. As these transformations occur, the ability of forests to provide ecosystem services will change.

The extent of change will likely depend on the severity of the realized climate change. Thus, to understand the potential impacts on ecosystem services, multiple climate change

scenarios representing a range of severities should be considered. We use three in our case study: one scenario in which climate change is ignored, "None"; one in which climate change is predicted to be mild, "Ensemble RCP 4.5" (also "E45"); and one in which climate change is predicted to be severe, "Ensemble RCP 8.5" (also "E85"). These scenarios differ in their assumption of the additional energy per unit area that will be absorbed by the atmosphere, a value known as radiative forcing (RF). E45 assumes an RF of 4.5 W/m^2 and E85 assumes 8.5 W/m^2. In general, larger values of RF correspond to more severe climate change.

A given value of radiative forcing does not map to a single prediction of climate change, because researchers may disagree in how the climate will respond to that amount of RF. This is why for a given RF numerous climate models exist. A common approach to handling the disagreement among the climate models is to use an ensemble of climate models that all assume the same RF. We adopt this approach here for our E45 and E85 scenarios.

Each of these scenarios corresponds to an ensemble of 17 climate models. These climate models originate from the Fifth Assessment (AR5) on climate performed by the Intergovernmental Panel on Climate Change (IPCC). The selection and assembly of the 17 climate models used in these ensembles was conducted by Cookston (2016) and the Climate-FVS team [7].

The other scenario, None, ignores any effects of climate change. While the number of studies incorporating climate change is increasing, this is still a common assumption in modern studies such as Schroder *et al.* (2013) [20]. Because it has served as the basis for many past studies of ecosystem services, the None climate scenario serves as a control against which we will compare the other two.

Each climate scenario corresponds to a different parameterization of the model, since the vegetation, fuels, and sediment delivery data depend on climate. Thus, changing the climate scenario has the potential to affect the amount and location of NSO habitat, the effects of fuel removals on NSO habitat, the fire hazard of the Drink Area, the efficacy of the fuel removals in reducing fire hazard, and the sediment delivered as a result of fuel removals. This drives changes to the relationships among the ecosystem services as well, which we

Table 1.2: Summary of the performance of the efficient frontiers for each climate change scenario.

		None	**E45**	**E85**
Fire hazard	min	21321.21	23219.82	23268.02
	avg	21406.26	23324.41	23369.57
	max	21933.29	23973.79	23724.98
NSO habitat	min	2532.33	2412.18	2171.10
	avg	2536.31	2447.92	2421.99
	max	2540.05	2477.18	2481.01
Sediment delivery	min	0	0	0
	avg	10.25	27.98	31.19
	max	24.57	63.43	69.68

investigate using the aforementioned conflict measures.

1.3.5 Results

We parameterized and solved the multi-objective model (equations (1.22)-(1.36)) for each of the climate scenarios, generating three efficient frontiers: Z_{None}, Z_{E45}, and Z_{E85} for the None, Ensemble RCP 4.5, and Ensemble RCP 8.5 scenarios, respectively. Z_{None} consists of 51 solutions, Z_{E45} consists of 701 solutions, and Z_{E85} consists of 1083. Figure 1.11 shows the frontiers in their 3-dimensional objective spaces while Figure 1.12 provides a single parallel coordinates plot with all frontiers. The summary details of their objective achievements are listed in Table 1.2.

Individual provision of ecosystem services

The average achievement of all ecosystem services decreases with increasing severity of climate change – see Table 1.2. We find that the difference in ecosystem service provision is

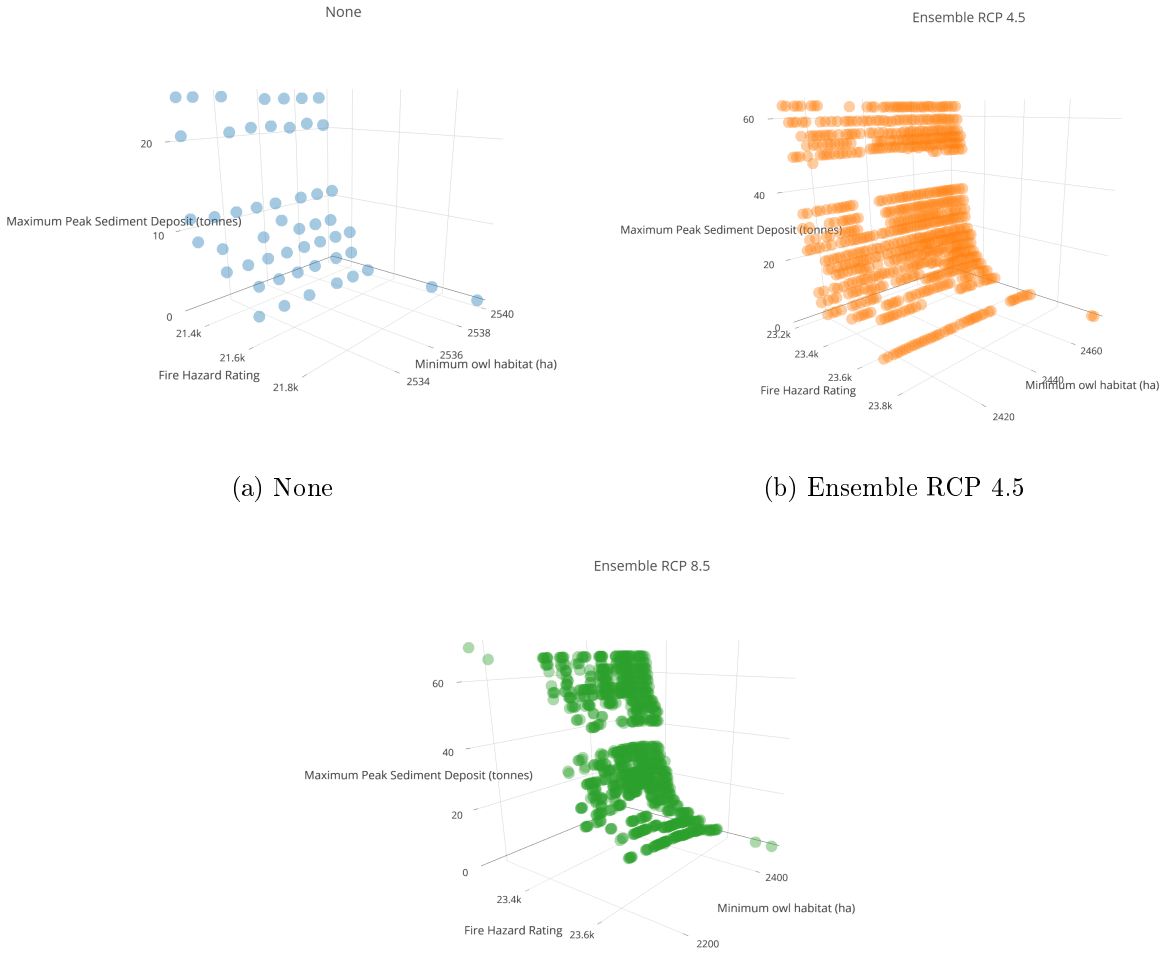

(a) None

(b) Ensemble RCP 4.5

(c) Ensemble RCP 8.5

Figure 1.11: Efficient frontiers for each climate change scenario.

greater between the assumption of no climate change and mild climate change (None to E45) than it is between mild climate change and severe climate change (E45 to E85).

Sediment delivery All scenarios have a lower bound on sediment delivery of 0, but the upper bound and the average sediment delivery both increase with climate change severity. Compared to the None scenario with an average sediment delivery of 10.25 tonnes, the

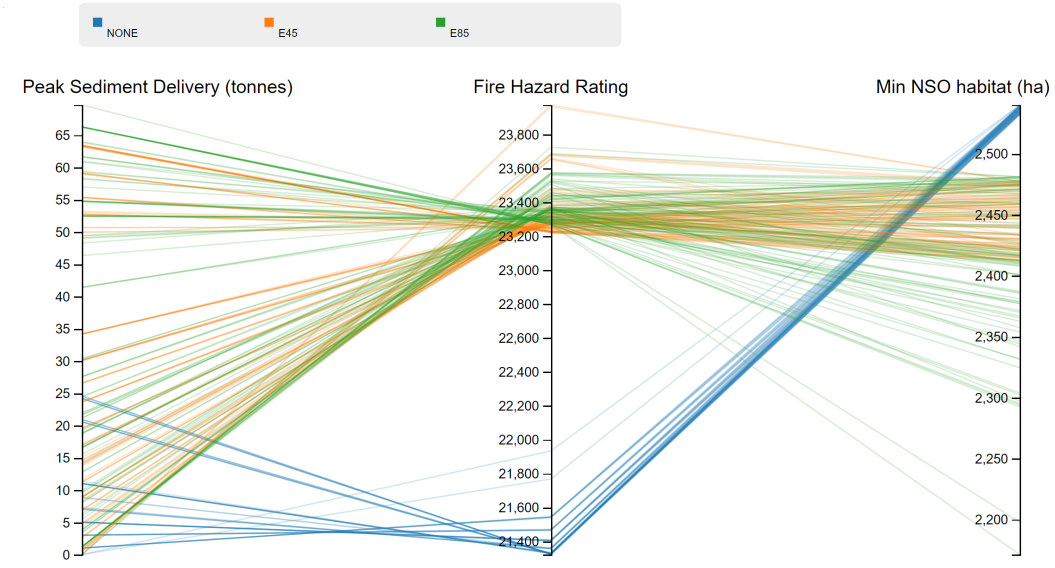

Figure 1.12: Parallel coordinates view of the frontiers. Each axis represents an ecosystem service optimized by the model and each line represents a solution. In all objectives, we notice that None appears to outperform both the E45 and E85 scenarios, which show similar average objective achievements. To increase visual clarity, only a subset of solutions for E45 and E85 are shown.

average amount of sediment delivered in E45 is 27.98 tonnes, an increase of 172%. The average for E85 is 31.19 tonnes, 204% higher than None.

Fire hazard Similarly, we find that the average fire hazard of the Drink Area increases with climate change severity. The average for None is 21406.26 while E45 and E85 both perform approximately 9% worse with an average of 23324.41 and 23369.57, respectively.

NSO habitat Finally, we also observe a decrease in the average provision of NSO habitat with increasing climate change. Compared to None which has an average provision of 2536.31 ha of NSO habitat, the average provision in the E45 scenario is 88.4 ha less (-3.5%), and E85 is 114.3 ha less (-4.5%).

We also find that for the sediment delivery and NSO habitat objectives, the range of achievable values increases with climate change severity. For sediment delivery, the range

Table 1.3: Hypervolume for each climate change scenario. Hypervolume values increase with increasing severity of climate change.

	None	**E45**	**E85**
Hypervolume	0.876977	0.866857	0.829541

increases from 24.57 tonnes in None to 63.43 in E45 to 69.68 in E85. And for NSO habitat, the range increases from 7.72 ha in None to 65 ha in E45 and to 309.91 ha in E85.

Conflict and the joint provision of ecosystem services

As we saw for provision of individual ecosystem services, our results show that climate change will have an impact on conflict and the joint provision of ecosystem services as well.

We observe a decreasing hypervolume with increasing severity of climate change – see Table 1.3. The hypervolume for E45 is 0.0101 less than None, and E85 is 0.0474 less than None. However, all hypervolumes indicate frontiers which fill a large percentage of the objective space, as the smallest value (E85) is $I_{H1}(Z_{\text{E85}}) = 0.8295$. The binary hypervolumes (see Table 1.4) tend to align with the hypervolumes, with larger values of $I_{H2}(Z_1, Z_2)$ when $I_{H1}(Z_1) > I_{H1}(Z_2)$ and smaller values when $I_{H1}(Z_2) > I_{H1}(Z_1)$. We note that no frontier is dominated by any other, as all values in Table 1.4 are strictly positive.

Sediment delivery-NSO Habitat In the pairwise comparison of objectives, we observe little conflict between sediment delivery and NSO habitat under all climate scenarios. This is evident first in the proposed conflict metric C_{ij}, for which the largest value across all frontiers is 0.25 – see Table 1.5. We also notice the lack of conflict in Figure 1.13. The figure shows the efficient frontier plotted in the sediment delivery-NSO habitat plane, where each objective has been normalized such that better values are higher and worse values are lower. For instance, in this graph, the point $(1, 1)$ represents 0 sediment delivery and maximum NSO habitat. For all climate scenarios, we see similar uniform spreads of solutions as well

Table 1.4: Binary hypervolumes for each pair of climate scenarios. No values are negative, indicating that no frontiers are dominated by another and that all frontiers uniquely enclose some volume of the objective space.

Z_1	Z_2	$I_{H2}(Z_1, Z_2)$
None	**E45**	0.026154
None	**E85**	0.058001
E45	**None**	0.016034
E45	**E85**	0.045156
E85	**None**	0.010565
E85	**E45**	0.007841

Table 1.5: Conflict between sediment delivery and NSO habitat across climate scenarios.

	C_{ij}	$c_{ij,\rho}$	$c_{ij,d}$
None	0.19639	0.3974	0.4942
E45	0.25667	0.5194	0.4941
E85	0.19284	0.5160	0.3737

as multiple solutions near the sub-dimensional ideal solution at $(1, 1)$.

NSO habitat-fire hazard According to C_{ij}, the conflict between NSO habitat and fire hazard is again small for all climate scenarios; however, it appears to decrease with increasing severity of climate change. We see in Table 1.6 that the average distance to the ideal decreases with increasing severity of climate change. See also Figure 1.14 which shows spreads of solutions for each climate scenario in the NSO habitat-fire hazard plane. The solutions are increasingly more clustered near the sub-dimensional ideal solution with increasing climate change severity.

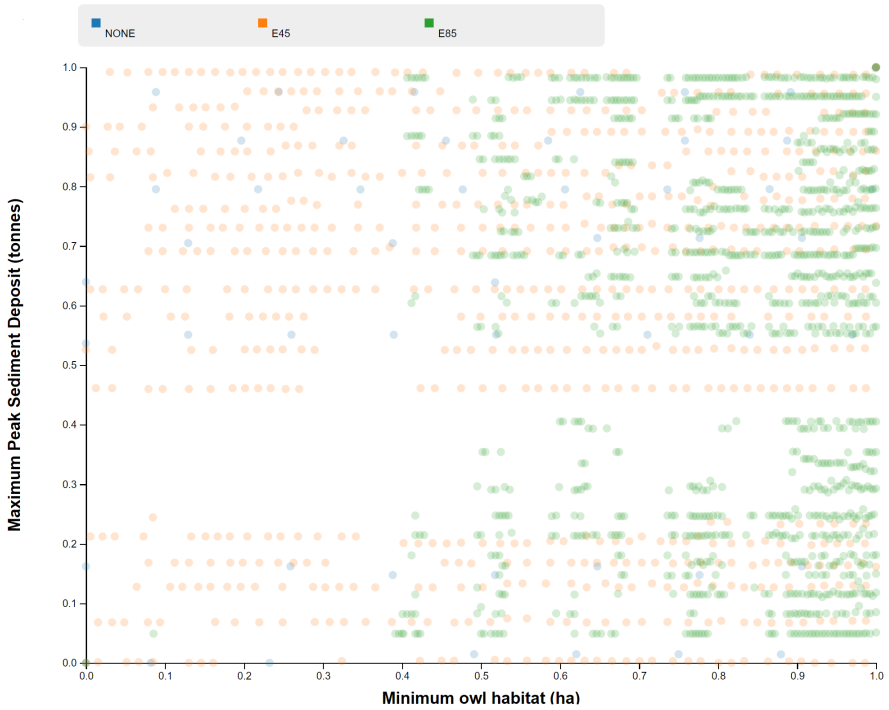

Figure 1.13: NSO habitat versus sediment delivery for all climate scenarios. No obvious conflict pattern exists between the objectives in any climate scenario.

Fire hazard-sediment delivery In all climate scenarios, the strongest pairwise conflict is between fire hazard and sediment delivery. This is apparent from both Figure 1.15 and the conflict metric, Table 1.7. All rank correlation conflict values $c_{ij,\rho} > 0.95$, indicating strong negative rank correlation. In Figure 1.15 we observe a clear void of solutions in all climate change scenarios near the sub-dimensional ideal solution at $(1, 1)$; this is unlike Figures 1.13 and 1.14. We also notice that the None and E45 solutions generally extend beyond the E85 solutions in this plane.

1.3.6 Discussion

We divide our discussion of results into three sections: first, the decreasing provision of individual ecosystem services with climate change; second, the increase in the number of solutions and in the range of NSO habitat available; and third, conflict and the joint provision

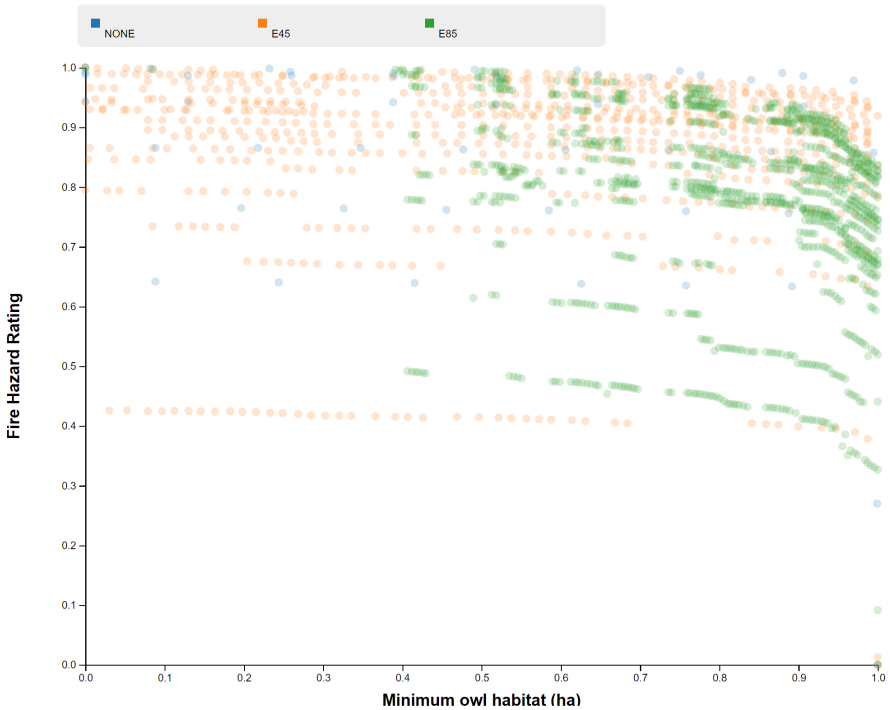

Figure 1.14: NSO habitat versus fire hazard for all climate scenarios.

of ecosystem services.

Decreasing provision of individual ecosystem services

We observe decreasing provision of individual ecosystem services with increasing severity of climate change. In particular, we see that the difference between no climate change (None) and mild climate change (E45) was greater than the difference between mild climate change (E45) and severe climate change (E85). Refer to Table 1.2. This suggests that, at least for the ecosystem services in this study, the realization of climate change is more significant than the severity of that change.

Sediment delivery Investigating the cause of the degradation in objective provision, we find for sediment delivery that the average amount of sediment delivered per fuel removal increases with climate change. See Figure 1.16. The average sediment delivery per fuel

Table 1.6: Conflict between NSO habitat and fire hazard across climate scenarios.

	C_{ij}	$c_{ij,\rho}$	$c_{ij,d}$
None	0.25805	0.6622	0.3897
E45	0.20560	0.5807	0.3541
E85	0.15670	0.6643	0.2359

Table 1.7: Conflict between sediment delivery and fire hazard across climate scenarios.

	C_{ij}	$c_{ij,\rho}$	$c_{ij,d}$
None	0.36039	0.9927	0.3630
E45	0.36097	0.9853	0.3664
E85	0.38261	0.9514	0.4021

removal under E45 is nearly twice the sediment delivery under the None scenario (81% higher), and the E85 scenario is 0.4% higher than that. This is driven by two underlying factors: the response in sediment delivery to prescribed burns and the frequency with which prescribed burns are assigned[2]. Our simulations show that increasing the severity of climate change causes pronounced increases in sediment delivery as a result of prescribed burns. We also find that relative to the None scenario, prescribed burns are assigned more frequently in the climate change scenarios – 8 times more frequently in E45 and 10.1 times more frequently in E85. See Table 1.8. These effects combine to produce the result seen in Figure 1.16 of sediment delivery levels that increase with climate change severity.

Fire hazard For the fire hazard objective, we first note that the increase in fire hazard with climate change severity is not simply due to the model selecting less area for treatment. This value is essentially constant across both treatment periods and all climate scenarios –

[2]For additional information on how stands are assigned a specific fuel removal technique such as thinning or prescribed burn, see the appendix, §A.

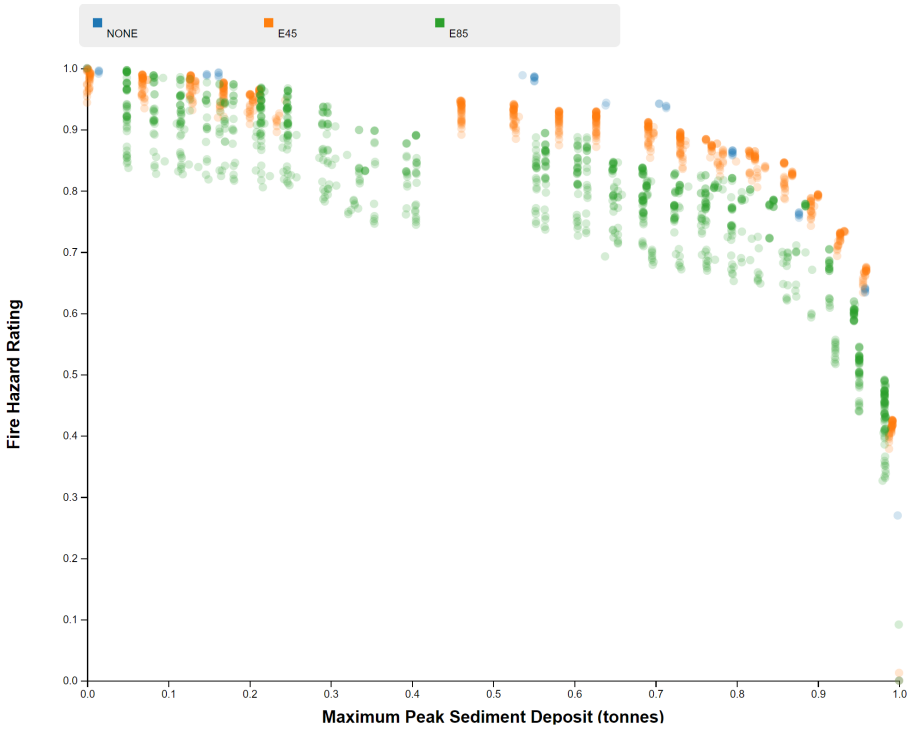

Figure 1.15: Sediment delivery versus fire hazard for all climate scenarios.

see Table 1.9. Instead, we find that the increase in fire hazard is due to the impact of climate change on the fuel model classification of the stands in the Drink Area. In E45 and E85, more stands are assigned a fuel model classification that is associated with higher fire hazard (refer to Table 1.1 for the mapping from fuel models to fire hazard). This is shown in Figure 1.17, where we observe a larger percentage of stands having a fire hazard rating of either 4 or 5 under the E45 and E85 scenarios than in None.

NSO habitat Lastly, we find that the decrease in NSO habitat is largely due to the effects of climate change on the vegetation in the Drink Area. Recall that of the criteria used to determine if a stand qualifies as NSO habitat, two of them are determined by vegetation characteristics: the presence of at least one tree with DBH $>$ 76 cm and canopy closure of at least 60%. While climate change has minimal impact on the former, the average canopy

Table 1.8: Frequency and impact of prescribed burns for each climate scenario. The combination of more frequent prescribed burns and increased sediment delivery per prescribed burn results in the higher values of sediment delivery in E45 and E85 observed in Figure 1.16.

	None	**E45**	**E85**
Average sediment delivery (tonnes) from prescribed burn	31.23	48.56	48.97
Number of prescribed burns assigned	34	272	344

Table 1.9: Areas treated per period across climate scenarios. The values are nearly constant for both periods and for each climate scenario.

	None	**E45**	**E85**
Area treated (ha) in period 1	2427.31	2426.90	2414.58
Area treated (ha) in period 2	2427.56	2427.71	2427.63

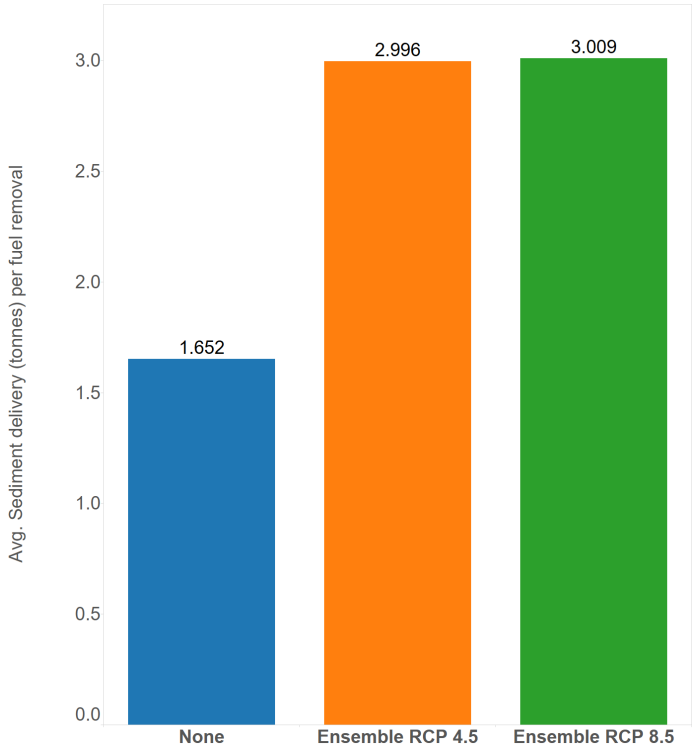

Figure 1.16: Average spike in sediment delivery as a result of performing fuel removals for each climate change scenario.

closure for stands in the Drink Area decreases with increasing severity of climate change. See Figure 1.18.

Variation in number of solutions and range of values for NSO habitat

With increasing climate change severity, we noted an increase in the number of solutions generated by our model: 51 for Z_{None}, 701 for Z_{E45}, and 1083 for Z_{E85}. We speculate that the cause of this is the same as that of the increase in the range of NSO habitat provided – the impact of fuel removals on whether a stand qualifies as NSO habitat.

We see in Table 1.10 the number of instances in which performing a fuel removal disqualifies a stand from being NSO habitat. Let us refer to such a fuel removal as a "disqualifying treatment." We notice that disqualifying treatments occur more than twice as frequently in

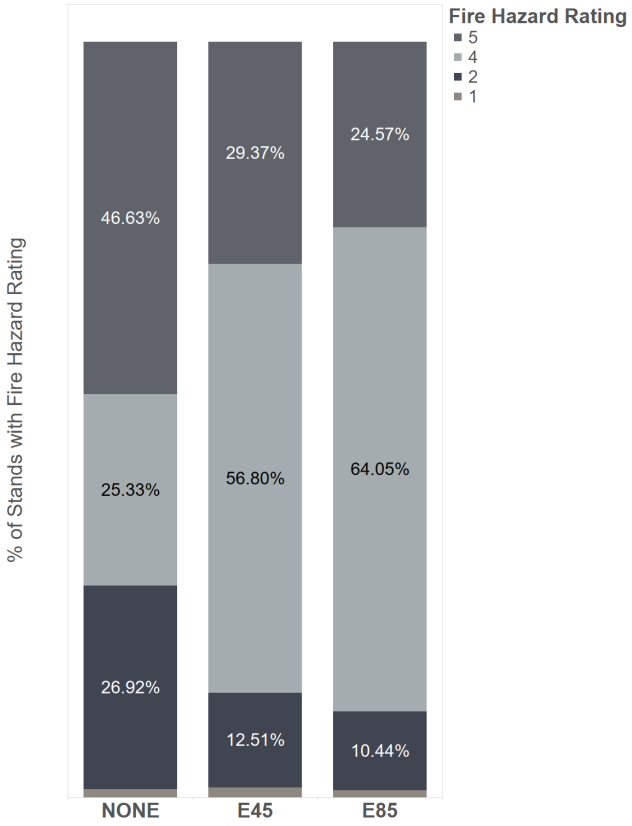

Figure 1.17: Distributions of fire hazard ratings across the Drink Area under each climate change scenario. Moving from left to right (in increasing climate change severity), we observe an increase in the percent of stands classified with more extreme fire hazards (ratings of 4 and 5).

E45 and E85 than in None. To understand why the increase in the number of disqualifying treatments increases the number of solutions, consider a stand i which is suitable NSO habitat under all fuel removal schedules r in the None scenario. Then the values of sediment delivery and fire hazard would vary with selection of r, but the resulting NSO habitat would always be the same. Now, in the case of climate change (say E45) some fuel removal schedules r are disqualifying treatments. That is, the selection of r also now changes whether stand i qualifies as NSO habitat. This influences the objective function value via equation (1.25), and it also affects the clustering associated with that stand (constraints (1.28) and

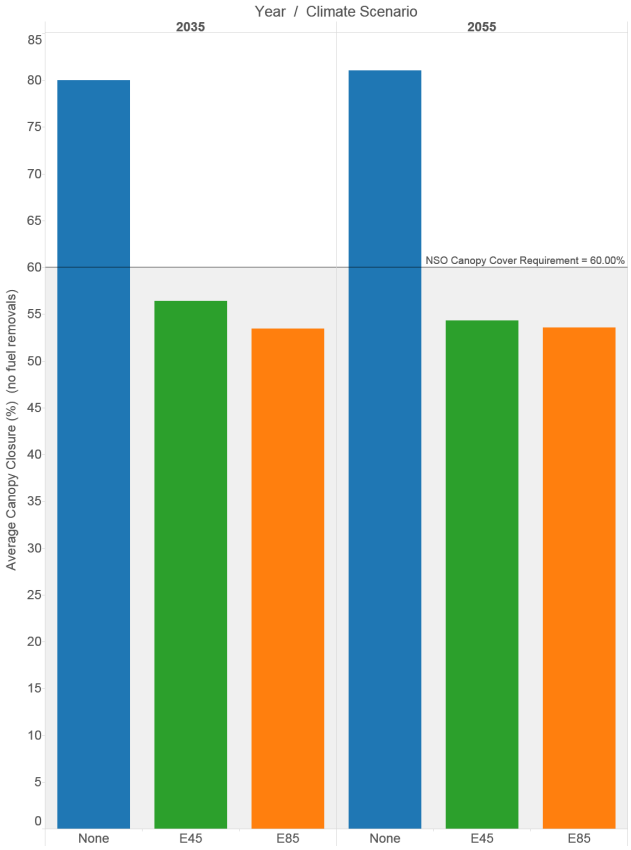

Figure 1.18: Average canopy closure for stands in the Drink Area for each climate scenario. Shown are canopy closure values during years 2035 and 2055 (the years in which NSO habitat is measured) when no fuel removals are performed. We see that with increasing climate change severity, canopy closure decreases.

(1.29)). This leads to solutions that did not exist in None.

If the disqualifying treatments generated little fire hazard reduction in return for the disqualification of NSO habitat, then these decisions would not be part of the optimal solutions $\mathbf{x} \in P$. However, we also find that the reduction in fire hazard for a given disqualifying treatment increases with climate severity (Figure 1.19). This leads to greater incentive for the model to sacrifice NSO habitat in favor of fire hazard reduction.

Together, these factors lead to an increase in the number of solutions as well as greater diversity in the total amount of NSO habitat provided by the models.

Table 1.10: Shown here are the number of times for each climate scenario that a fuel removal triggers the disqualification of a stand from being NSO habitat.

Climate change scenario	**Disqualifications of NSO habitat as a result of fuel removals**
None	24
Ensemble RCP 4.5	63
Ensemble RCP 8.5	67

Conflict and the joint provision of ecosystem services

We observe a decreasing hypervolume with increasing climate change severity. Lower values for the hypervolume are indicative of more conflict, meaning that climate change induces more conflict among the ecosystem services and leads to less joint provision of objectives.

The difference in hypervolume between None and E45 $I_{H1}(Z_{\text{None}}) - I_{H1}(Z_{\text{E45}}) \approx 0.01$. Recall that a difference of h in hypervolumes equates to a difference of $h^{1/M}$ in each objective (Figure 1.2). Thus, despite the small size of the difference between $I_{H1}(Z_{\text{None}})$ and $I_{H1}(Z_{\text{E45}})$, it signifies an additional joint provision of objectives of approximately 21.6%. This difference is greater between None and E85, approximately 0.05, representing an additional joint provision of ecosystem services of approximately 36.2%.

From the hypervolumes alone, it is uncertain whether None represents a strictly better frontier than either E45 or E85 or if, despite their smaller hypervolume values, E45 and E85 enclose some region of the objective space that is not enclosed by None. Any such region would extend further into the objective space, representing the presence of solutions that achieve greater joint provision of ecosystem services. The results of the binary hypervolume were presented in Table 1.4.

The results show that no frontier is dominated by any other, and each frontier encloses some region of the objective space not enclosed by the others. For the pairs of frontiers for which the binary hypervolume is greatest ($(Z_{\text{None}}, Z_{\text{E85}})$ and $(Z_{\text{E45}}, Z_{\text{E85}})$), this additional

extension into the objective space is most obvious in Figure 1.15. We see for values of sediment delivery between 0.15 and 0.8 that None appears to dominate E45 which appears to dominate E85. Further, for sediment delivery values between 0.8 and 1, it appears that E45 dominates E85 and None, between which any domination relationship is difficult to discern.

The existence of these areas leads to the lower value of conflict C_{ij} between sediment delivery and fire hazard in None and E45 than in E85. We note the success of the conflict metric C_{ij} here: all frontiers in the sediment delivery-fire hazard plane of Figure 1.15 are similar. They have similar shape and achievement towards the sub-dimensional ideal solution, yet the metric is able to distinguish differences in conflict between them.

For the other pairwise objective comparisons, as we saw in Figures 1.13 and 1.14, the distribution of solutions more closely resembles a uniform two-dimensional scattering. There is no clear conflict pattern between them like that which we saw in Figure 1.15. As a result, C_{ij} reports little conflict between these objective pairs, as desired. However it varied in unexpected ways between the climate scenarios. In these cases, we find that the distance component $c_{ij,d}$ was primarily responsible for the variations, as the rank correlations tended to be insignificantly different from 0.5. It appears the conflict metric C_{ij} is susceptible to such variations when neither the $c_{ij,d}$ nor $c_{ij,\rho}$ component tends towards their limiting values of 0 and 1.

However, in general, we find our process of utilizing the hypervolume measures and the proposed conflict metric to have been successful in quantifying conflict within and among the frontiers. The pairwise conflict metric successfully identified the pair of objectives which demonstrated the most conflict, and the hypervolumes indicated which climate scenarios allow for greater joint provision of ecosystem services.

1.4 General Discussion & Conclusion

We used a case study of the impact of climate change on the joint provision of forest ecosystem services to successfully demonstrate the utility of a new measure of pairwise objective conflict

and to demonstrate a new application of existing conflict measures in the quantification of conflict within and among multi-objective systems.

We argue that this case study served as a rigorous first test of the conflict measures and conflict quantification process, because there was little overall conflict in these systems and the differences in relative objective achievement across climate scenarios were not great. For instance, in the case study, the hypervolume for each climate scenario was relatively large, with solutions occupying over 80% of the objective space in all cases. In addition, in all but one pairwise objective comparison, it was difficult to discern any distinct conflict relationship between the objectives. As a result, our proposed conflict metric and the hypervolume indicators were required to detect subtle differences in conflict, which they did successfully. Should the differences in objective achievement between climate scenarios have been more pronounced, or should the objectives have been in greater conflict with one another, we suspect the utility of these measures and the process we demonstrated here would only increase.

Of course, our success here is not a guarantee of future success. In consideration of different climate change scenarios, different ecosystem services, or a different study area, the conflict measures may prove less useful. The application of this quantitative conflict analysis should be tested in other multi-objective systems as well.

Consider again the manager of the food processing facility, this time with looming regulatory changes on the horizon, such as a change in the maximum allowable microbiological levels. For a number of such levels, the manager may consider the balance in processing time and nutrient retention. Would the hypervolumes report greater joint objective provision under larger allowable levels? Would this reported decrease in conflict be an accurate assessment of reality? In the case of the manager overseeing multiple hospitals, how might the pairwise conflict between operating cost and patient throughput vary between them?

Based off our results, we believe that our new conflict measure and the process we suggest would be useful to the managers in these cases as well. As we saw in the case study, the proposed conflict measure was successful in being able to identify which objective pairs were

most in conflict. We also saw that the hypervolumes were successful in detecting increasing system-level conflict under different environmental conditions. These variations in conflict were supported by the underlying model data.

However, the new conflict metric and process are not without shortcomings. We first note that C_{ij} is susceptible to relatively large variations in cases where neither the distance component $c_{ij,d}$ nor the rank correlation component $c_{ij,\rho}$ tend toward their $[0, 1]$ bounds. In these cases, the components have more influence on the value of the conflict metric C_{ij}, so slight variations can lead to relatively large differences. In addition, differences in system conflict cannot be totally explained by the collection of pairwise conflict measures. For instance, while the small pairwise conflict metrics in the case study (< 0.4) coarsely correspond to large hypervolumes (> 0.8), we cannot use them to explain the source of the small differences observed in hypervolume. In fact, for the climate scenario with the most system conflict, E85, the sum of its pairwise conflict metrics was smallest. Lastly, the conflict measures used in the proposed process can be difficult to interpret, since they provide results in terms of relative objective achievement. That is, instead of having results that are measurable in the dimensions of the objectives, they are instead in percent achievements for the objectives.

In summary, we have provided a foundation for quantitative conflict analysis for the comparison of multi-objective systems. Our results show that our proposed process and the new conflict metric are successful in quantifying and differentiating the amount of conflict within and across multi-objective systems and that they stand to serve as a useful tool for multi-objective decision making. However, more experimentation with the proposed quantitative conflict analysis is required to better understand the limitations of its utility, and refinements to the new pairwise conflict measure should be investigated. Especially useful refinements would be those which address the variation in the conflict metric when neither component tends towards a limiting value of 0 or 1.

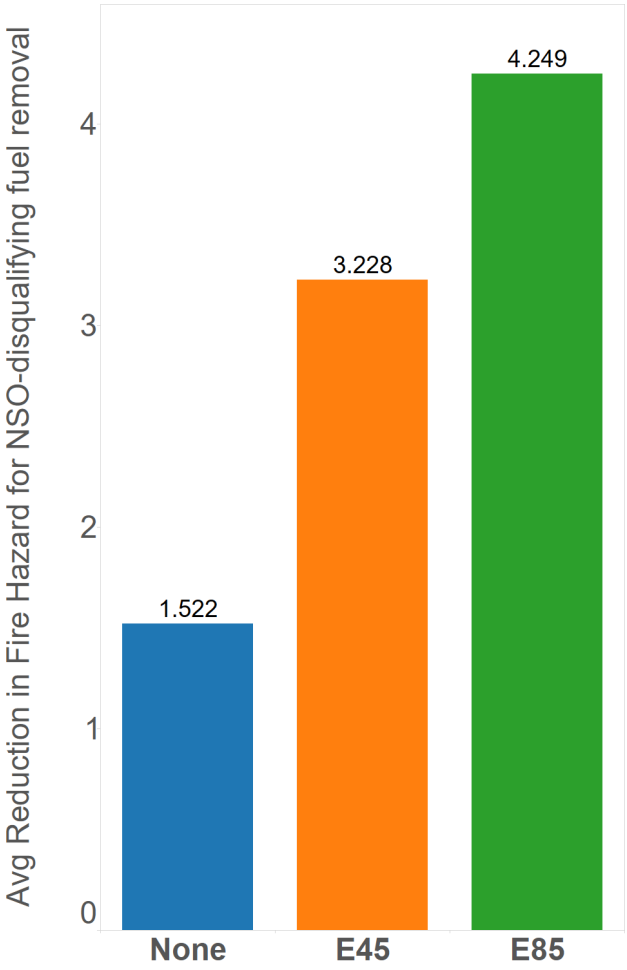

Figure 1.19: Some stands may always be NSO habitat and others may never be NSO habitat, regardless of model decisions. For those stands which vary based on model decisions, we see here the average efficacy of fuel removals which disqualify their being NSO habitat. This value increases with increasing climate change, indicating greater incentive for the model to forgo NSO habitat in favor of fire hazard reduction.

BIBLIOGRAPHY

[1] Hal E Anderson. Aids to determining fuel models for estimating fire behavior. *The Bark Beetles, Fuels, and Fire Bibliography*, page 143, 1982.

[2] Monica L Bond, RJ Gutiérrez, Alan B Franklin, William S LaHaye, Christopher A May, and Mark E Seamans. Short-term effects of wildfires on spotted owl survival, site fidelity, mate fidelity, and reproductive success. *Wildlife Society Bulletin*, pages 1022–1028, 2002.

[3] Dimo Brockhoff and Eckart Zitzler. Are all objectives necessary? on dimensionality reduction in evolutionary multiobjective optimization. In *Parallel Problem Solving from Nature-PPSN IX*, pages 533–542. Springer, 2006.

[4] Dimo Brockhoff and Eckart Zitzler. Objective reduction in evolutionary multiobjective optimization: Theory and applications. *Evolutionary Computation*, 17(2):135–166, 2009.

[5] US Congress. Endangered species act. *Washington DC*, 1973.

[6] Steven P Courtney and Andrew B Carey. *Scientific evaluation of the status of the Northern Spotted Owl*. Sustainable Ecosystems Institute Portland, OR, 2004.

[7] Nicholas Crookston. Details of data and methods used for calculating future climate estimates, 2016.

[8] Nicholas Crookston. Get climate-fvs ready data, 2016.

[9] Kalyanmoy Deb and D Saxena. Searching for pareto-optimal solutions through dimensionality reduction for certain large-dimensional multi-objective optimization problems. In *Proceedings of the World Congress on Computational Intelligence (WCCI-2006)*, pages 3352–3360, 2006.

[10] James R Frankenberger, Shuhui Dun, Dennis C Flanagan, Joan Q Wu, and William J Elliot. Development of a gis interface for WEPP model application to great lakes forested watersheds. In *International Symposium on Erosion and Landscape Evolution (ISELE), 18-21 September 2011, Anchorage, Alaska*, page 139. American Society of Agricultural and Biological Engineers, 2011.

[11] Tomas Gal and Heiner Leberling. Redundant objective functions in linear vector maximum problems and their determination. *European Journal of Operational Research*, 1(3):176–184, 1977.

[12] Jaime R. Goode, Charles H. Luce, and John M. Buffington. Enhanced sediment delivery in a changing climate in semi-arid mountain basins: Implications for water resource management and aquatic habitat in the northern rocky mountains. *Geomorphology*, 139âĂŞ140(0):1 – 15, 2012.

[13] Anke K Hutzschenreuter, Peter AN Bosman, and Han La PoutrÚ. Evolutionary multiobjective optimization for dynamic hospital resource management. In *International Conference on Evolutionary Multi-Criterion Optimization*, pages 320–334. Springer, 2009.

[14] George G Ice, Daniel G Neary, and Paul W Adams. Effects of wildfire on soils and watershed processes. *Journal of Forestry*, 102(6):16–20, 2004.

[15] Louis R Iverson and Anantha M Prasad. Predicting abundance of 80 tree species following climate change in the eastern united states. *Ecological Monographs*, 68(4):465–485, 1998.

[16] Evangelos Kanoulas and Javed A Aslam. Empirical justification of the gain and discount function for ndcg. In *Proceedings of the 18th ACM conference on Information and knowledge management*, pages 611–620. ACM, 2009.

[17] Prasad Karande and Shankar Chakraborty. Application of multi-objective optimization on the basis of ratio analysis (moora) method for materials selection. *Materials & Design*, 37:317–324, 2012.

[18] Jay OâĂŹLaughlin. Conceptual model for comparative ecological risk assessment of wildfire effects on fish, with and without hazardous fuel treatment. *Forest Ecology and Management*, 211(1):59–72, 2005.

[19] Robin C Purshouse and Peter J Fleming. Conflict, harmony, and independence: Relationships in evolutionary multi-criterion optimisation. In *International Conference on Evolutionary Multi-Criterion Optimization*, pages 16–30. Springer, 2003.

[20] Svetlana A (Kushch) Schroder, Sándor F Tóth, Robert L Deal, and Ettl Gregory J. Multi-objective optimization to evaluate tradeoffs among forest ecosystem services following fire hazard reduction in the Deschutes National Forest, USA. *Ecosystem Services*, Special Issue "Integrated Valuation of Ecosystem Services: Challenges and Solutions", accepted.

[21] José Oscar H Sendín, Antonio A Alonso, and Julio R Banga. Efficient and robust multi-objective optimization of food processing: A novel approach with application to thermal sterilization. *Journal of Food Engineering*, 98(3):317–324, 2010.

[22] Sándor Tóth. *Modeling Timber and Non-timber Trade-offs in Spatially-Explicit Forest Planning*. PhD thesis.

[23] Sándor F Tóth, Gregory J Ettl, Nóra Könnyű, Sergey S Rabotyagov, Luke W Rogers, and Jeffrey M Comnick. Ecosel: multi-objective optimization to sell forest ecosystem services. *Forest Policy and Economics*, 35:73–82, 2013.

[24] James M Vose, David Lawrence Peterson, Toral Patel-Weynand, et al. *Effects of climatic variability and change on forest ecosystems: a comprehensive science synthesis for the US forest sector*. US Department of Agriculture, Forest Service, Pacific Northwest Research Station Portland, OR, 2012.

[25] Yu Wang, Hailian Yin, Shuai Zhang, and Xiongqing Yu. Multi-objective optimization of aircraft design for emission and cost reductions. *Chinese Journal of Aeronautics*, 27(1):52–58, 2014.

[26] Lyndon While, Philip Hingston, Luigi Barone, and Simon Huband. A faster algorithm for calculating hypervolume. *IEEE transactions on evolutionary computation*, 10(1):29–38, 2006.

[27] Eckart Zitzler. *Evolutionary algorithms for multiobjective optimization: Methods and applications*, volume 63. Citeseer, 1999.

[28] Eckart Zitzler, Lothar Thiele, Marco Laumanns, Carlos M Fonseca, and Viviane Grunert Da Fonseca. Performance assessment of multiobjective optimizers: an analysis and review. *Evolutionary Computation, IEEE Transactions on*, 7(2):117–132, 2003.

Appendix A

TREATMENT SPECIFICATIONS FOR THE DRINK AREA

Table A.1 provides a mapping from a stand's vegetation conditions to the treatment action to apply to the stand. If a stand's conditions do not correspond to any row in the table, then no action is taken. The table was adapted from Schroder [20]. The plant association groups in the Drink area are shown in Figure A.1.

Table A.1: Rules governing treatment assignments.

SDI[1]	**CBD**[2]	**TPH**$_{<18}$[3]	**Fuel model**[4]	**BA**$_{\text{MHD+WF},>46}$[5]	**Treatment**
Lodgepole pine (LPD) plant association					
< 87	N/A	N/A	N/A	N/A	**Prescribed burn**
≥ 87	> 0.037	> 49	≥ 10	N/A	**Thin, pileburn slash and fuels**[6]
			< 10	N/A	**Thin, pileburn slash**
Mixed conifer wet (MCW) or mountain hemlock (MHD) plant associations					
< 87	N/A	N/A	N/A	N/A	**Prescribed burn**

[1]Stand Density Index, calculated in metric units (trees per ha).

[2]Crown bulk density (kg/m^3)

[3]Number of trees per hectare whose diameter at breast height (DBH) is less than 18 cm

[4]According to the Anderson rating system[1]

[5]Basal area in m^2 of all mountain hemlock (MHD) and white fir (WF) trees with DBH $> 46cm$.

[6]Pileburning slash involves removal of thinned trees only, while pileburning slash and fuels also involves removal of materials that were on the ground before thinning (Wall, Powers, 2012; personal communication)

≥ 87	> 0.037	> 49	$= 10$	> 7.5	**Thin, pileburn slash and fuels, prescribed burn**
				≤ 7.5	**Thin, pileburn slash and fuels**
			> 10	N/A	**Thin, pileburn slash and fuels**
			< 10	N/A	**Thin, pileburn slash**
		≤ 49	$= 10$	≥ 7.5	**Prescribed burn**
	≤ 0.037	N/A	$= 10$	≥ 7.5	**Prescribed burn**
	N/A	N/A	$\in \{6, 8, 9, 10\}$	N/A	**Prescribed burn**[7]
Mixed conifer dry (MCD) plant association					
< 87	N/A	N/A	N/A	N/A	**Prescribed burn**
≥ 87	> 0.037	> 49	$\in \{10, 11\}$	N/A	**Thin, pileburn slash and fuels, prescribed burn**
			≥ 12	N/A	**Thin, pileburn slash and fuels**
			< 10	N/A	**Thin, pileburn slash**
		≤ 49	$\in \{10, 11\}$	N/A	**Prescribed burn**
	≤ 0.037	N/A	$\in \{10, 11\}$	N/A	**Prescribed burn**
	N/A	N/A	$\in \{6, 8, 9, 10\}$	N/A	**Prescribed burn**[7]

[7] Only if prescribed burn was assigned in period 1 (applies to period 2 treatment assignments only)

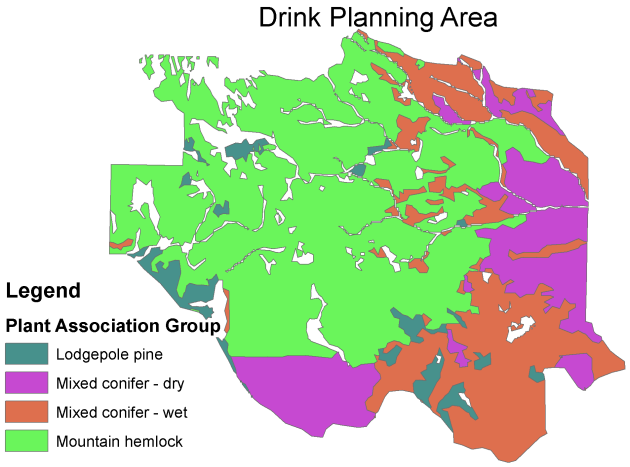

Figure A.1: Plant association groups in the Drink Area that are considered for treatments.